Journal of Structural Dynamics, 3, (pp. 1-29) 2024
AMPIE: Added Mass Passive Input Estimation - Acquiring Driving Points without Direct Excitation

AMPIE: Added Mass Passive Input Estimation - Acquiring Driving Points without Direct Excitation

Benjamin Kammermeier [*1,2], Johannes Mayet [†1], and Daniel J. Rixen [‡2]

[1] *BMW, Research and Development, Schleißheimer Str. 422, 80788 München, Germany*
[2] *TUM, Chair of Applied Mechanics, Boltzmannstraße 15, 85748 Garching bei München, Germany*

Abstract

Experimental and hybrid substructuring allow the virtual analysis of complex structures that are rather represented by experimental models than simulations. Coupling the experimental models with other structures requires adequate *driving points* — generally described by six degrees of freedom with three translations and rotations with forces and torques as inputs as well as translational and angular accelerations as outputs. However, the measurement of these driving points is challenging. In particular, experimentally acquiring all six inputs causes the main effort. For example, excitation devices that directly exert a torque are not widely applicable or three translational directions are not accessible. Therefore, adapter structures are frequently used in practice, which increase the experimental effort or can be impractical due to a lack of space and reachability. The proposed strategy is the replacement of active excitation devices, i.e. impulse hammers or shakers, on the driving points, by passive, rigid bodies, simply referred to as masses. Compared to the existing mass uncoupling method which is also based on this fundamental idea, the main improvement is a simplified notation that enables the incorporation of data from multiple masses and parametric state-space systems. The main finding is that the proposed strategy is suited to estimate driving point dynamics that allow to predict the effect of assembled structures on channels that were not used in the estimation of the driving point, indicating the physical relevance of the estimated dynamics.

Keywords: Substructuring, Mass Uncoupling Method, AMPIE, Parametric Systems, Input Estimation

Received on September 15, 2023, Accepted on October 5, 2024, Published on October 17, 2024

Nomenclature

Abbreviations

AMPIE	Added Mass Passive Input Estimation
FRF	Frequency Response Function
IRLS	Iterative Reweighted Least Squares
LES	Linear Equation System
MUM	Mass Uncoupling Method
NP	Non-Parametric
NP-FRF	Non-Parametric Frequency Response Function
VPT	Virtual Point Transformation

Matrices, Operators, Indices

$\boldsymbol{i}$	Complex number
$\mathbb{R}^{n\times m}$	Real n-by-m matrix
$\mathbb{C}^{n\times m}$	Complex n-by-m matrix
$0_{n\times m}\in\mathbb{R}^{n\times m}$	n-by-m nullmatrix
$I_n \in \mathbb{R}^{n\times n}$	n-by-n identity matrix
:	Subscript for all rows
$^+$	Pseudo inverse
$\tilde{}$	Measured quantity
*	Predicted quantity
ω	Frequency

[*] benjamin.kammermeier@bmw.de
[†] johannes.mayet@bmw.de
[‡] rixen@tum.de

i	Index for driving points
k	Index for frequency ω_k
$\Omega \in \mathbb{R}^{n_\omega \times 1}$	Frequency grid
n_ω	Number of frequencies
j	Index for masses

Inputs, Outputs, Dimensions

$z \in \mathbb{C}^{n_z \times 1}$	Reference inputs
$p \in \mathbb{C}^{n_p \times 1}$	Reference outputs
$u_i \in \mathbb{C}^{6 \times 1}$	Inputs at driving point i
$y_i \in \mathbb{C}^{6 \times 1}$	Outputs at driving point i
$\tilde{u}_i \in \mathbb{C}^{n_I^i \times 1}$	Measured inputs at driving point i
$\tilde{y}_i \in \mathbb{C}^{n_O^i \times 1}$	Measured outputs at driving point i
$z^+ \in \mathbb{C}^{n_{z^+} \times 1}$	Additional reference inputs in test-case
n_z	Number of reference inputs
n_p	Number of reference outputs
n_I^i	Number of measured inputs at driving point i
n_O^i	Number of measured outputs at driving point i
N	Number of driving points i
n_{z^+}	Number of test-case inputs

Systems, Dimensions, Transformations

$G \in \mathbb{C}^{n_O \times n_I}$	System for substructuring
n_O	Number of outputs of G
n_I	Number of inputs of G
$G_{pz} \in \mathbb{C}^{n_p \times n_z}$	Reference channels
$G_{y_i u_i} \in \mathbb{C}^{6 \times 6}$	Coupling channels at driving point i
$G_{:z} \in \mathbb{C}^{n_I \times n_z}$	Submatrix of G with inputs z
$G_{:u_i} \in \mathbb{C}^{n_I \times 6}$	Submatrix of G with inputs u_i
$\tilde{G} \in \mathbb{C}^{\tilde{n}_O \times \tilde{n}_I}$	System with measured inputs $\tilde{u}_i$ and measured ouputs $\tilde{y}_i$
$\tilde{n}_O$	Number of outputs of $\tilde{G}$
$\tilde{n}_I$	Number of inputs of $\tilde{G}$
$T_I^i \in \mathbb{R}^{n_I^i \times 6}$	Transformation from $\tilde{u}_i$ to u_i
$T_O^i \in \mathbb{C}^{6 \times n_O^i}$	Transformation from $\tilde{y}_i$ to y_i
$T_O \in \mathbb{R}^{n_O \times \tilde{n}_O}$	Output-transformation from $\tilde{G}$ to G
$T_I \in \mathbb{R}^{\tilde{n}_I \times n_I}$	Input-transformation from $\tilde{G}$ to G

AMPIE - NP-FRF, Single Mass

$G^i \in \mathbb{C}^{n_O \times n_I}$	G with mass at driving point i
$G_{:z}^i \in \mathbb{C}^{n_O \times n_z}$	Submatrix of G^i with inputs z and mass at driving point i
$M \in \mathbb{R}^{6 \times 6}$	Representation of mass
$m \in \mathbb{R}^{1 \times 1}$	Translational inertia
$J \in \mathbb{R}^{3 \times 3}$	Rotational inertia
$\boldsymbol{M}_i \in \mathbb{R}^{n_I \times n_O}$	Force-feedback at driving point i
$\Delta G^i \in \mathbb{C}^{n_O \times n_z}$	Left-hand side of NP-FRF-based LES for driving point i
$G_M^i \in \mathbb{C}^{6 \times n_z}$	Right-hand side of NP-FRF-based LES for driving point i

AMPIE - Multiple Masses

$M_j \in \mathbb{R}^{6 \times 6}$	j-th coupled mass
n_M	Number of masses at each driving point i
$G^{ij} \in \mathbb{C}^{n_O \times n_I}$	G with mass j at driving point i
$G_{:z}^{ij} \in \mathbb{C}^{n_O \times n_z}$	Submatrix of G^{ij} with inputs z and mass j at driving point i
$\boldsymbol{M}_{ij} \in \mathbb{R}^{n_I \times n_O}$	Force-feedback at driving point i of mass j
ΔG^{ij}	Left-hand side of NP-FRF-based LES for driving point i and mass j, $\Delta G^{ij} \in \mathbb{C}^{n_O \times n_z}$
G_M^{ij}	Right-hand side of NP-FRF-based LES for driving point i and mass j, $G_M^{ij} \in \mathbb{C}^{6 \times n_z}$

AMPIE - State-Space, Predictions, Test-Case

n	Number of states
$A \in \mathbb{R}^{n \times n}$	State-space state matrix
$B \in \mathbb{R}^{n \times n_I}$	State-space input matrix
$C \in \mathbb{R}^{n_O \times n}$	State-space output matrix
$D \in \mathbb{R}^{n_O \times n_I}$	State-space feedthrough matrix
$\Lambda(\omega) \in \mathbb{C}^{n \times n}$	Frequency-dependent part of state-space FRF
$B_{:z}, B_{:u_i}$	Submatrices of input matrix B
$\otimes$	Kronecker product
$\downarrow$	Vectorization of matrix
$b_{ij} \in \mathbb{C}^{n_O n_z \times 1}$	Right-hand side of state-space-based LES for driving point i, mass j at freqeuncy ω
$A_{ij} \in \mathbb{C}^{n_O n_z \times 6n}$	Left-hand side of state-space-based LES for driving point i, mass j at freqeuncy ω
$x_i \in \mathbb{R}^{6n \times 1}$	Unknown of state-space-based LES for driving point i
W_k^R	Weighting matrix for real part at frequency ω_k, $W_k^R \in \mathbb{R}^{n_O n_z \times n_O n_z}$
W_k^I	Weighting matrix for imaginary part at ω_k, $W_k^I \in \mathbb{R}^{n_O n_z \times n_O n_z}$
$A_{ij}^{\blacksquare} \in \mathbb{R}^{6n \times 6n}$	Weighted left-hand side for driving point i and mass j
$b_{ij}^{\blacksquare} \in \mathbb{R}^{6n \times 1}$	Weighted right-hand side for driving point i and mass j
$A_i^{\blacksquare} \in \mathbb{R}^{6n \times 6n}$	Left-hand side for driving point i and all masses
$b_i^{\blacksquare} \in \mathbb{R}^{6n \times 1}$	Right-hand side for driving point i and all masses
$G_{:z}^{ij,\star}$	Predicted system for j-th mass at driving point i for inputs z, $G_{:z}^{ij,\star} \in \mathbb{C}^{n_O \times n_z}$
G^+	System G with input z^+ for test-case, $G^+ \in \mathbb{C}^{n_O \times (n_I + n_{z^+})}$
G^{test}	Measured reference for test-case, $G^{test} \in \mathbb{C}^{n_O \times (n_z + n_{z^+})}$
$G^{test,\star}$	Prediction for test-case, $G^{test,\star} \in \mathbb{C}^{n_O \times (n_z + n_{z^+})}$

1 Motivation, Related Work and Contribution

Motivation Experimental or hybrid substructuring allow the virtual analysis of complex structures. The vibroacoustic analysis and optimization of e.g. a full vehicle cannot be achieved by pure simulation, as the dynamical properties are too complex to be captured numerically. Instead, the idea of substructuring starts with an experimental model of the complex structure. Other structures from experiments or simulation can be coupled virtually to the experimentally obtained model. Solely using experimental models is termed as experimental substructuring, adding also simulation-based models is termed as hybrid substructuring. The virtual prediction of the assembled system allows for example to find optimized vibroacoustical properties. Such properties could be the vibration at the steering wheel as output due to road noise on the vehicle's wheel suspension as input. These quantities are not involved but affected by the coupling procedure. In this contribution such quantities are referred to as reference inputs and reference outputs.

The coupling of models requires precise information about the driving point dynamics at the interface, which is in general found to be difficult to measure [1]. The measurement of a structure typically consists of two parts: acceleration as outputs and forces as inputs. A mechanical connection at a sufficiently rigid location of the specimen is described by six degrees of freedom, including three translations and three rotations with forces and torques as inputs and translational and angular accelerations as outputs, which fully describe the rigid body motion. In practice, this can for example be the vicinity of a screw hole in a car body where other structures can be mounted. In this contribution, these inputs and outputs are referred to as coupling inputs and coupling outputs which form a 6-by-6 driving point. An illustration for a generic example is given in Figure 1.

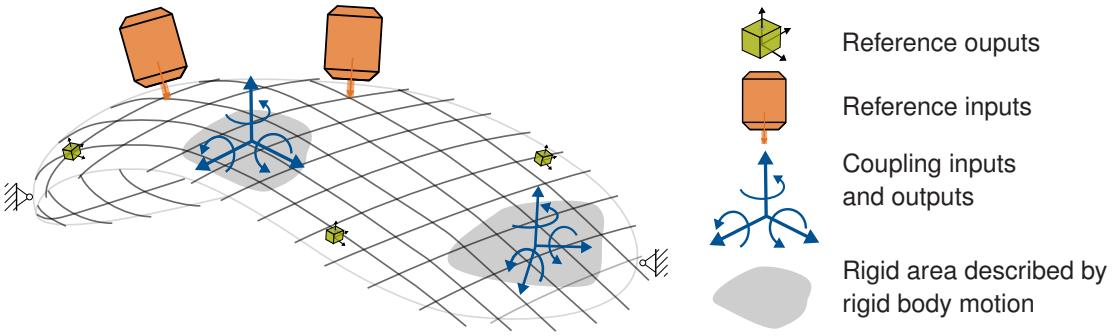

Fig. 1: Generic example of a system for substructuring with two reference inputs in orange, symbolized by shaker devices, nine reference outputs from three triax accelerometers in green, and two 6-by-6 driving points to couple models of other substructures symbolized by blue coordinate systems.

However, off-the-shelf devices only allow the recording of translational accelerations and forces. For the case of outputs, the commonly used triax accelerometers give access to all three translations. In contrast, translational inputs are mostly recorded in a single direction via impulse hammers or shaker devices. Compared to the outputs, accessing all translational input forces can already be cumbersome, e.g. for plane structures. Furthermore, torques are in practice mostly applied using adapter structures as devices that directly exert a torque are not widely applicable. Therefore, for the described application of experimental substructuring, obtaining the driving point *inputs* is the main challenge. This issue is addressed by the AMPIE strategy which is subsequently put into context by a brief overview of existing approaches for related problems.

Related Work One set of strategies to access unmeasured quantities is based on numerical finite element models of the experimentally analyzed specimen. Measurements are typically considered to encompass the true structural properties, whereas finite element models give a fine spatial resolution, including rotations, but require assumptions which lead to an imperfect representation of the investigated system. Expansion techniques, such as SEREP [2], VIKING [3], SEMM [4, 5], or the recently proposed method in [6] typically use experimentally obtained information and enforce it to the numerical model. The experimentally described channels are typically not altered, thereby expanding the measurement to the numerical resolution. Similarly, model updating [7, 8, 9] combines experimental and numerical information. However, in case of model updating, the experimental data is typically used to tune parameters in the numerical model, which will not result in a perfect reproduction of the experimental channels. Since the approach

outlined in this paper is supposed to remain purely experimental, these methods are not considered further.

A purely experimental approach to access driving point outputs and in particular inputs is based on adapter structures. Early on, the application of rigid masses was put forward in [10] where the acceleration information on the rigid mass is fitted to the required six degrees of freedom via least-squares. The undesired mass is numerically removed, but inputs, i.e. forces and torques, are not considered. Still, this method can be seen as precursor of subsequently introduced adapter-based approaches. In [11], the mass uncoupling method (MUM) is used to access torque inputs based on the moment of inertia of an attached T-block where specific sensor and excitation positions on the T-block are used. Similar to other approaches [12], the feedback equation is solved in a scalar fashion which is an important difference to the proposed AMPIE scheme. In [13], the T-block method is extended to an arbitrary number of inputs and outputs on the T-block which is numerically considered as a finite element model. The idea is similar to the method described by Allen et al. in [14] which is known as the transmission simulator [15]. The approaches have in common that an adapter structure is mounted on the system and used to access output rotations [10] , torque inputs [11, 13], or a generalized interface force and displacement [14, 15]. However, the excitation of that adapter structure is still required in all cases [11, 13, 14, 15].

Regardless of the application of an adapter structure, experimental approaches require methods to estimate rotations from translational information. The previously discussed approach [10] uses a rigid mass to fit translational accelerations on six rigid body modes, giving rotation information. The finite difference approach, for example discussed in [16, 17], provides information for rotations or torques based on a set of output or input locations. Depending on the number of sensors, this method allows to use higher orders of the underling finite difference, however, the interpolation requires the sensors to be in line. In contrast, the virtual point transformation (VPT) [18, p. 57] blends the entire geometrical information, locations and directions, of given outputs and inputs together in one transformation. As its application is straightforward, the VPT is also used in the present strategy. In this context, it is worth to mention that the VPT was recently extended to include data from rotational accelerometers [19], yielding improved results. Note that this extension is limited to rotation outputs. The direct measurement of rotation inputs, i.e torques, was investigated, see e.g. [20, 21, 22]. However, no currently used approach of direct torque excitation with practical relevance is known to the authors.

The fundamental idea of the present contribution is that attaching a mass and observing the resulting change in the dynamical properties of the structure allow the replacement of an active excitation at the driving point. The same idea is the basis for MUM which was used in different scenarios, such as estimating torque inputs based on a T-block in [11], to determine unmeasured columns of the FRF (Frequency-Response Function) in [23], or for the compensation of sensor mass-loading in [12]. The most important difference to the present approach is the mathematical formulation. In [23, 11, 12], the equations of the coupled systems are treated in a scalar fashion and solved one after another, not in a matrix-based formulation that is put forward in this contribution. The flexibility that is obtained by the proposed, matrix-based rearrangement yields the possibility to deal in a straightforward manner with a full 6-by-6 driving point, multiple attached masses, and to use capabilities of system identification and parametric systems. In the present case, the parametric systems are denoted as first order state-space models that essentially consist of modal parameters. In order to better grasp the differences in the proposed and previous formulations, a brief comparison of both calculations for a scalar driving point is given in Appendix B.

Among others, the MUM approach was used to cancel sensor mass-loading [12]. In the area of sensor mass-loading, further ideas related to the present contribution were proposed in the literature. For example, in [24] multiple masses are considered. In [25], uncertainty is considered for the estimation of auto-FRFs using a maximum likelihood estimator. Both aspects are combined in this contribution, as uncertainty is tackled by the intentional use of multiple masses to further overdetermine the set of equations and to, thereby, reduce the impact of noise.

Contribution The proposed strategy is denoted as Added Mass Passive Input Estimation (AMPIE), where the term passive refers to the absence of active excitation devices at the driving points of interest. In summary, the main features of this contribution are

- a simple feedback-based derivation,
- the possibility to accommodate multiple masses, increasing the available information,
- the seamless consideration of a 6-by-6 driving point,

- the extension to parametric systems, decreasing the number of unknowns.

It must be noted that there are further approaches that seek to estimate unmeasured data based on a given set of measurements. A comprehensive overview is not the purpose of this work. Still, some approaches that do not entirely fit in the above categorization are mentioned. For example, [26] shows that, theoretically, the orthogonality of normal modes would be sufficient to reconstruct the entire FRF matrix from one row or column. The round trip theory [27] can be used to reconstruct the auto FRF at a passive interface, given excitation on both sides and output measurements on one side of that interface.

From a practical point of view, the proposed strategy can exhibit several benefits in an actual experimental procedure. The envisaged example is the experimental, vibroacoustic optimization of a vehicle where several 6-by-6 driving points over and within the specimen are to be determined to tune the dynamic behavior by adding subcomponents. The possible drawbacks of standard, adapter-based strategies can be

- the application of an impulse hammer is limited, e.g. due to reachability issues, or a possible lack of space for the impact motion, or not possible, e.g. inside a passenger compartment where required closed doors make the application infeasible,
- the application of an inertial shaker inside the passenger compartment will generate spurious acoustic sources and deteriorate acoustic measurements,
- the experimental (de)mounting effort for adapter structures and inertial shakers becomes large for multiple driving points; for arbitrary positions on the specimen it is physically demanding and potentially not possible,
- the assembly of adapter and shaker can become voluminous, potentially resulting in reach- and accessibility issues,
- a numerical decoupling procedure is required since the adapter alters the specimen.

In addition, once the driving points are experimentally determined, the reliability of the obtained data and the accuracy of subsequent predictions remain questionable. The easiest way to test this is the coupling of a mass, experimentally and numerically, and to compare the results. This validation procedure alone provides the minimum information that is required to perform the AMPIE procedure in the first place.

Outline The mathematical formalism for the AMPIE scheme is derived in Section 2. At first, the required system representations and quantities are introduced. Based on this overview, the mathematical details of the AMPIE procedure are outlined. In order to increase the amount of experimentally obtained data and to mitigate the impact of noise, the application of multiple masses per driving points is discussed. For the same reason, the strategy is derived for parametric systems along with required weighting techniques. Parametric and non-parametric strategies are compared, and the concept of predictions and test-cases which are used to assess the AMPIE strategy are outlined. In Section 3, an experimental example is introduced that is used to show the applicability of the outlined scheme. The results are discussed in Section 4. A conclusion and outlook on further work is given in Section 5.

2 Theoretical Derivation

The theoretical derivation is separated into several steps. The generic example from Figure 1 is used to illustrate the most important quantities. First, in Section 2.1, the basic system representation for substructuring G is introduced along with the system $\tilde{G}$ which is the outcome of the typical measurement strategy. With both systems introduced, the difference of the standard measurement approach to the AMPIE strategy is explained using the generic example. The mathematical details of the AMPIE strategy are subsequently explained in Section 2.2 where the fundamental, mass-induced feedback equation is rearranged and the unknown, required quantities are isolated. The idea to use multiple masses is put forward and derived for the case of non-parametric FRF (NP-FRF). Third, in Section 2.3, the solution process for parametric systems is described. In Section 2.4, a summary is given and the concepts of predictions and test-cases are introduced. These concepts are subsequently used to assess the proposed strategy.

2.1 Structural Measurement and Quantities of Interest

Representation for Substructuring At first, the motivating idea for experimental or hybrid substructuring from Section 1 is re-examined and extended by the required formal notation. In order to identify a complex structure experimentally, such that other experimental- or simulation-based models can be coupled, reference in- and outputs as well as coupling in- and outputs are required. Considering vehicle-vibroacoustics as example, the analysis typically takes place in frequency domain. Accordingly, the fundamental system representation is the FRF $G(\omega) \in \mathbb{C}^{n_O \times n_I}$ where $\mathbb{C}^{n_O \times n_I}$ is the space of complex matrices, ω is the frequency, n_I and n_O are the number of all in- and outputs, respectively. However, note that the frequency-dependency will mostly be omitted, particularly within equations, to avoid unnecessary long terms. Taking into account the outlined model structure, the FRF G can be denoted as

$$\begin{pmatrix} p \\ y_1 \\ \vdots \\ y_N \end{pmatrix} = \underbrace{\begin{bmatrix} G_{pz} & G_{pu_1} & \dots & G_{pu_N} \\ G_{y_1 z} & G_{y_1 u_1} & \dots & G_{y_1 u_N} \\ \vdots & \vdots & \ddots & \vdots \\ G_{y_N z} & G_{y_N u_1} & \dots & G_{y_N u_N} \end{bmatrix}}_{=G} \begin{pmatrix} z \\ u_1 \\ \vdots \\ u_N \end{pmatrix} \tag{1}$$

where the described quantities are the reference outputs $p(\omega) \in \mathbb{C}^{n_P \times 1}$ and inputs $z(\omega) \in \mathbb{C}^{n_Z \times 1}$ as well as the coupling outputs and inputs $y_1(\omega), u_1(\omega), ..., y_N(\omega), u_N(\omega) \in \mathbb{C}^{6 \times 1}$. The number of driving points is N. The frequency-dependency will again be omitted for compactness.

Each pair $y_i = \begin{pmatrix} y_i^x & y_i^y & y_i^z & y_i^\alpha & y_i^\beta & y_i^\gamma \end{pmatrix}^\mathsf{T}$, $u_i = \begin{pmatrix} u_i^x & u_i^y & u_i^z & u_i^\alpha & u_i^\beta & u_i^\gamma \end{pmatrix}^\mathsf{T}$ fully describes the rigid body motion of driving point i where the superscripts x, y, and z denote translational, the superscripts α, β, and γ rotational quantities in the chosen coordinate system for driving point i. The defined quantities are illustrated in Figure 2 for the generic example introduced in Figure 1.

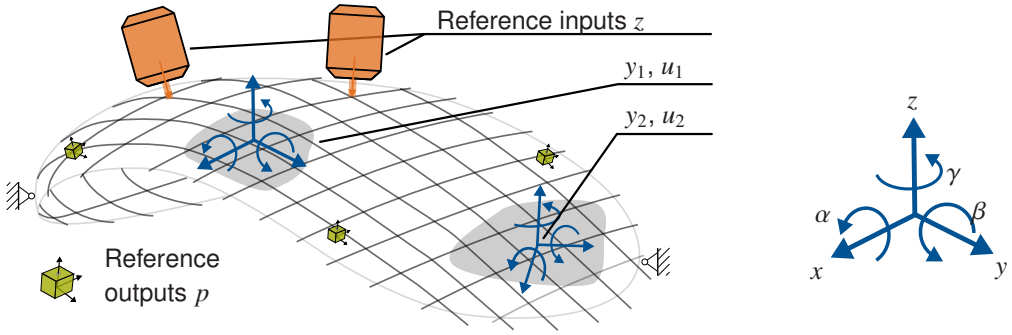

Fig. 2: Generic example of system G with two reference inputs z, nine reference outputs p, and two 6-by-6 driving points, y_1, u_1 and y_2, u_2 with three translations x, y, and z as well as three rotations α, β, and γ, to couple models of other structures.

The submatrices $G_{pz} \in \mathbb{C}^{n_p \times n_z}$ from Equation (1) form the reference channels, which are an important indicator for the outlined substructuring application: other structures can be coupled virtually on y_i and u_i, however, this coupling is only useful if the influence on G_{pz} is predicted correctly which strongly depends on the experimentally obtained quantities for y_i, u_i which form the coupling channels $G_{y_i u_i} \in \mathbb{C}^{6 \times 6}$. The effect of a coupled structure at $G_{y_i u_i}$ on G_{pz} and on all other driving points of the system is described by the remaining cross-channels, for example G_{pu_1}, $G_{y_2 z}$ or $G_{y_2 u_1}$. All these quantities are involved to come to a useful prediction of G_{pz} when a structure is coupled. The reference channels are the most suited channels to assess the outlined strategy, since

- they are by definition the quantities of interest and typically not involved in the coupling procedure,
- accurate predictions for the reference channels requires accurate estimates for the entire system – coupling and cross-channels – and therefore allow the assessment of all involved quantities.

Therefore, the assessment of the AMPIE strategy will focus on the reference channels and the adequate prediction of the effect of coupled structures on these channels.

For the AMPIE strategy, G from Equation (1) is partitioned column-wise, namely

$$G = \begin{bmatrix} G_{:z} & G_{:u_1} & \dots & G_{:u_N} \end{bmatrix}, \quad G_{:z} = \begin{bmatrix} G_{pz} \\ G_{y_1 z} \\ \vdots \\ G_{y_N z} \end{bmatrix}, \quad G_{:u_i} = \begin{bmatrix} G_{pu_i} \\ G_{y_1 u_i} \\ \vdots \\ G_{y_N u_i} \end{bmatrix} \tag{2}$$

where the submatrices $G_{:z} \in \mathbb{C}^{n_O \times n_z}$ and $G_{:u_1}, ..., G_{:u_N} \in \mathbb{C}^{n_O \times 6}$ contain all outputs which is indicated by the colon-operator while the reference and coupling inputs are denoted separately. This notation already shows that AMPIE takes into account all measured outputs while z and u_i are treated separately. This is similar to the standard approach of structural measurements where one input is excited while all outputs are measured. The typical approach to these standard measurements is outlined subsequently to further highlight the differences and also benefits of the AMPIE strategy.

Standard Measurement Scenario As described in the introduction, in most practical applications u_i and y_i are not measured directly. Instead, outputs are obtained by triax acceleration sensors and inputs by shaker devices or impulse hammers exerting a force in a single direction. In order to reflect their close relation to u_i and y_i, the directly measured quantities associated with driving point i are denoted as $\tilde{y}_i \in \mathbb{C}^{n_O^i \times 1}$ and $\tilde{u}_i \in \mathbb{C}^{n_I^i \times 1}$, where n_I^i and n_O^i are the numbers of measured in- and outputs. In order to fully capture the rigid body motion, the forces $\tilde{y}_i$ are applied to an adapter structure. The generic example is adapted to this scenario in Figure 3 where the described quantities are included.

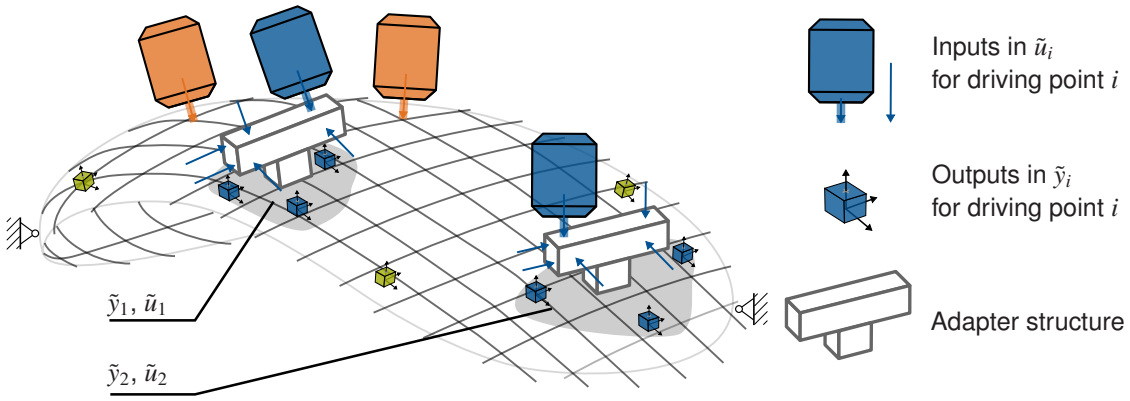

Fig. 3: Generic example of system $\tilde{G}$ with two reference inputs z, nine reference outputs p, two adapter structures at driving point 1 and 2 with three accelerometers, resulting in $\tilde{y}_1$ and $\tilde{y}_2$, and six force inputs on the adapter structure, resulting in $\tilde{u}_1$ and $\tilde{u}_2$, for each driving point.

As the driving point is described by a rigid body motion, the measured quantities $\tilde{y}_i$ and $\tilde{u}_i$ can be transformed into the required quantities u_i and y_i. In this contribution, the VPT is the method of choice to represent this step. Based on the location and orientation of sensors and exerted forces at driving point i, a transformation $T_O^i \in \mathbb{R}^{6 \times n_O^i}$ and $T_I^i \in \mathbb{R}^{n_I^i \times 6}$ can be defined such that $y_i = T_O^i \tilde{y}_i$ and $\tilde{u}_i = T_I^i u_i$, see [18, p. 57]. In practice, sufficient conditions to fully define this transformation are at least three triax accelerometers that are not located on a line, and at least two excitations in each spatial direction that are exerted at different locations. Therefore, excitations that are solely perpendicular to a plane are not sufficient which further explains the requirement of adapter structures. Using this transformation, the system $\tilde{G}$ based on $\tilde{u}_i$ and $\tilde{y}_i$ can be transformed into G:

$$\begin{pmatrix} p \\ \tilde{y}_1 \\ \vdots \\ \tilde{y}_N \end{pmatrix} = \underbrace{\begin{bmatrix} G_{pz} & \tilde{G}_{p\tilde{u}_1} & \dots & \tilde{G}_{p\tilde{u}_N} \\ \tilde{G}_{\tilde{y}_1 z} & \tilde{G}_{\tilde{y}_1\tilde{u}_1} & \dots & \tilde{G}_{\tilde{y}_1\tilde{u}_N} \\ \vdots & \vdots & \ddots & \vdots \\ \tilde{G}_{\tilde{y}_N z} & \tilde{G}_{\tilde{y}_N\tilde{u}_1} & \dots & \tilde{G}_{\tilde{y}_N\tilde{u}_N} \end{bmatrix}}_{=\tilde{G}} \begin{pmatrix} p \\ \tilde{u}_1 \\ \vdots \\ \tilde{u}_N \end{pmatrix} \Rightarrow G = \underbrace{\begin{bmatrix} I_{n_p} & 0 & \dots & 0 \\ 0 & T_O^1 & \dots & 0 \\ \vdots & \vdots & \ddots & \vdots \\ 0 & 0 & \dots & T_O^N \end{bmatrix}}_{T_O} \tilde{G} \underbrace{\begin{bmatrix} I_{n_z} & 0 & \dots & 0 \\ 0 & T_I^1 & \dots & 0 \\ \vdots & \vdots & \ddots & \vdots \\ 0 & 0 & \dots & T_I^N \end{bmatrix}}_{T_I} \tag{3}$$

The matrices T_O and T_I are obtained by stacking the transformations for each driving point in block-diagonal manner and by accounting for the reference channels with appropriate identity matrices $I_{n_p} \in \mathbb{R}^{n_p \times n_p}$ and $I_{n_z} \in \mathbb{R}^{n_z \times n_z}$ which are

of size n_p and n_z, respectively. Similar to Equation (2), the system $\tilde{G}$ can be partitioned according to

$$\tilde{G} = \begin{bmatrix} \tilde{G}_{:z} & \tilde{G}_{:\tilde{u}_1} & \dots & \tilde{G}_{:\tilde{u}_N} \end{bmatrix}, \text{ with: } G_{:z} = T_O \tilde{G}_{:z} \tag{4}$$

which will also be required in Section 2.2.

In order to further motivate the idea of AMPIE, the qualitative difference between in- and outputs is once more highlighted. First, the sensors to record the outputs are typically mounted to the specimen in a preparation step. The actual measurement procedure then consists of mounting a shaker device successively to all input locations in z, $\tilde{u}_1$, ..., $\tilde{u}_N$ which poses the main experimental effort — in particular when a large number of inputs must be measured to determine driving points for substructuring. Second, using standard triax accelerometers that are comparatively small to excitation devices, an adapter structure is mostly required for a well-defined VPT for the inputs. Considering this reasoning, the main experimental effort can be rephrased to obtaining $G_{:u_i}$ from Equation (1) which is ultimately obtained from $\tilde{G}_{:\tilde{u}_i}$ for each driving point according to $G_{:u_i} = T_O \tilde{G}_{:\tilde{u}_i} T_I^i$. This is the very quantity that results from the AMPIE strategy, which can simplify the required measurement procedure as explained next.

AMPIE As mentioned in Section 1, one drawback of the described adapter-based scenarios is the potential need for a numerical decoupling step as the mounted adapter structure alters the specimen. This alteration is the very effect that is used within the AMPIE strategy which is sketched in Figure 4 for the same generic example that was already outlined in Figures 2 and 3.

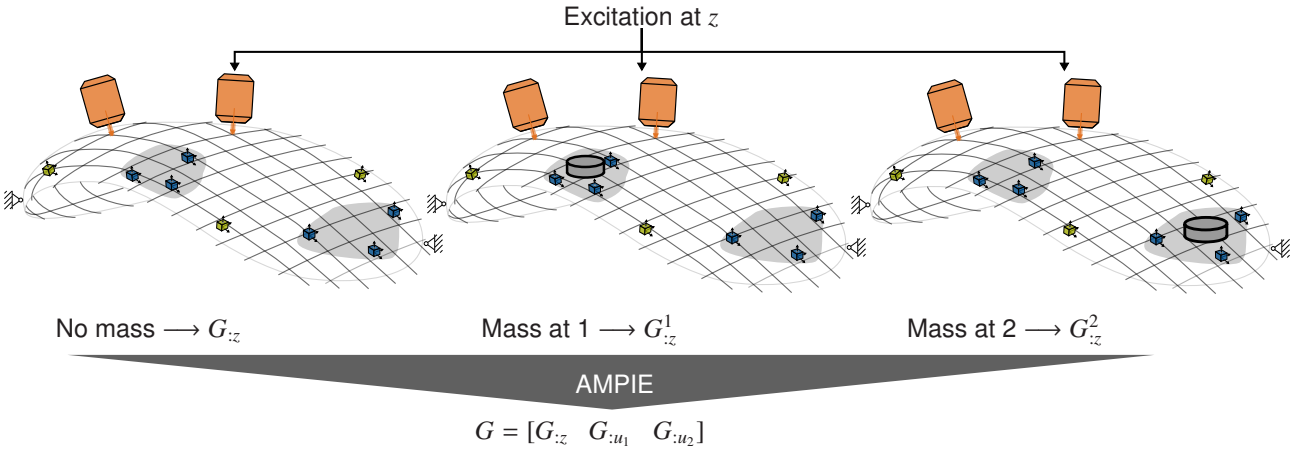

Fig. 4: Generic example of an experimental setting for substructuring approached with the AMPIE strategy where a mass is coupled to the driving points 1 and 2.

The decisive difference is that the specimen is only excited at the reference inputs z. An adapter structure with various excitation locations is not required at the driving points. Instead, the excitation at the reference inputs is applied to different systems. The difference between these systems is that a mass is coupled successively at the driving points of interest. Without any mass, the part $G_{:z}$ of the required system in Equation (1) is obtained. The systems $G^1_{:z}$ and $G^2_{:z}$ result from mounting a mass at driving point 1 and 2, respectively. In general, $G^i_{:z}$ is obtained when a mass is added at driving point i. Note that all these quantities are measured for the same inputs z and all outputs. The location of all used acceleration sensors is the same in all scenarios, therefore the dimension of the obtained quantities is the same: $G_{:z}, G^i_{:z} \in \mathbb{C}^{n_O \times n_z}$. Without loss of generality, the notation focuses on the system G. Note that all quantities in Figure 4 can be obtained from the measured outputs with the transformations $G_{:z} = T_O \tilde{G}_{:z}$ and $G^i_{:z} = T_O \tilde{G}^i_{:z} \quad \forall i \in \{1, ..., N\}$.

For the given example, only $G_{:z}$ from System (1) was actually measured, whereas $G_{:u_1}$ and $G_{:u_2}$, or more general $G_{:u_i}$, are not yet determined. The subsequently outlined formalism for the AMPIE approach shows that the given information is sufficient to determine the entire system G.

Summary Before the mathematical details are explained, a summary of the quantities that were discussed above is given below:

- The system representation for substructuring is given by G with reference outputs p and inputs z, and the coupling outputs y_i and inputs u_i that form 6-by6 driving points.

- The result of a standard measurement is given by $\tilde{G}$ with reference outputs p and inputs z, and the measured coupling outputs $\tilde{y}_i$ and inputs $\tilde{u}_i$, which can be transformed into G according to $G = T_O \tilde{G} T_I$. The main experimental effort is the excitation of coupling inputs and to obtain the submatrices $G_{:u_i} = T_O \tilde{G}_{:\tilde{u}_i} T_I^i$.
- In the AMPIE strategy, the quantities $G_{:u_i}$ are obtained mathematically based on the excitation of the reference channels z, i.e. $G_{:z}$, and by adding masses to the i-th driving point, resulting in $G^i_{:z}$.

2.2 Constant Feedback and Isolation of Unknowns

The goal of the standard measurement procedure in Figure 3 and the AMPIE strategy is to obtain the system G. As outlined above, the main idea of the AMPIE strategy is to replace the direct excitation at the driving point by attaching masses at the driving points of interest and only excite the resulting different systems at the reference inputs z. The mathematical formalism to calculate $G_{:u_1}, ..., G_{:u_N}$ from the given information $G_{:z}$ and $G^1_{:z}, ..., G^N_{:z}$ is derived in this section.

Starting with system G, a mass M at driving point i induces a constant feedback in the system. The added internal forces and torques are $u_i = My_i$ where the mass is defined as constant matrix $M \in \mathbb{R}^{6\times6}$, that can be defined for example according to Equation (30). The established feedback can be described by the well-known closed-loop equation for a constant feedback, see for example [28]. In order to capture that M only exerts a force u_i at driving point i and only depends on the acceleration y_i at driving point i, the corresponding channels must be selected by introducing the quantity $\boldsymbol{M}_i \in \mathbb{R}^{n_I \times n_O}$. The notation $0_{n_z \times n_p} \in \mathbb{R}^{n_z \times n_p}$ defines a nullmatrix of the indicated dimension. Using this definition, the feedback can be written as

$$G^i = (I - G\boldsymbol{M}_i)^{-1} G, \quad \boldsymbol{M}_i = \begin{array}{c} \begin{array}{ccccccc} & & & \text{Driving} & \text{Point} & \text{index:} & \\ & 1 & & \rightarrow & i & \rightarrow & N \end{array} \\ \begin{bmatrix} 0_{n_z\times n_p} & 0_{n_z\times 6} & \dots & 0_{n_z\times 6} & \dots & 0_{n_z\times 6} \\ 0_{6\times n_p} & 0_{6\times 6} & \dots & 0_{6\times 6} & \dots & 0_{6\times 6} \\ \vdots & \vdots & \ddots & \vdots & \iddots & \vdots \\ 0_{6\times n_p} & 0_{6\times 6} & \dots & M & \dots & 0_{6\times 6} \\ \vdots & \vdots & \iddots & \vdots & \ddots & \vdots \\ 0_{6\times n_p} & 0_{6\times 6} & \dots & 0_{6\times 6} & \dots & 0_{6\times 6} \end{bmatrix} \begin{array}{c} \\ 1 \\ \downarrow \\ i \\ \downarrow \\ N \end{array} \end{array} \tag{5}$$

which the basis to obtain $G_{:u_i}$. Recall that the systems G and G^i can be written as $G = \begin{bmatrix} G_{:z} & G_{:u_1} & \dots & G_{:u_N} \end{bmatrix}$ and $G^i = \begin{bmatrix} G^i_{:z} & G^i_{:u_1} & \dots & G^i_{:u_N} \end{bmatrix}$ which contain the submatrices $G_{:u_i}$ and $G^i_{:u_i}$. In the proposed method, only the submatrices $G_{:z}$ and $G^i_{:z}$ are obtained experimentally, whereas $G_{:u_i}$ and $G^i_{:u_i}$ are not known at this point. The main goal of the AMPIE scheme is to exploit Equation (5) to find $G_{:u_i}$.

An explicit expression of Equation (5) can be found for a one-dimensional coupling as discussed in Appendix B. However, if the additional mass introduces translational and rotational inertia in several directions, then Equation (5), in particular the inverse $(I - G\boldsymbol{M}_i)^{-1}$, cannot be solved in a straightforward fashion. Instead of solving the inverse in Equation (5), the formula is rearranged to isolate the unknown quantities and such that it can be solved for $G_{:u_i}$, based on the known quantities $G_{:z}$ and $G^i_{:z}$. This is achieved by the following steps:

$$\begin{aligned} G^i &= (I - G\boldsymbol{M}_i)^{-1} G \\ (I - G\boldsymbol{M}_i) G^i &= G \\ G^i - G\boldsymbol{M}_i G^i &= G \\ G^i - G &= G\boldsymbol{M}_i G^i \end{aligned} \tag{6}$$

The resulting Equation (6) allows two main steps to exclude unknown quantities and to isolate $G_{:u_i}$. First, systems G and G^i are separated in submatrices according to Equation (2) and (4). By multiplying an appropriate selection matrix

from the right, unknown quantities are eliminated:

$$\begin{aligned} G^i &- G &&= G\boldsymbol{M}_i\ G^i \\ \begin{bmatrix} G^i_{:z} & G^i_{:u_1} & \dots & G^i_{:u_N} \end{bmatrix} &- \begin{bmatrix} G_{:z} & G_{:u_1} & \dots & G_{:u_N} \end{bmatrix} &= G\boldsymbol{M}_i \begin{bmatrix} G^i_{:z} & G^i_{:u_1} & \dots & G^i_{:u_N} \end{bmatrix} \Big| \cdot \begin{bmatrix} I_z \\ 0 \\ \vdots \\ 0 \end{bmatrix} \\ G^i_{:z} &- G_{:z} &&= G\boldsymbol{M}_i\ G^i_{:z} \end{aligned} \tag{7}$$

In this expression, only the term $G\boldsymbol{M}_i$ still contains $G_{:u_i}$. To further isolate the items of interest, the second step exploits the structure of $\boldsymbol{M}_i$ and the row-wise partitioning of $G^i_{:z}$ according to Equation (2):

$$G\boldsymbol{M}_i G^i_{:z} = \begin{bmatrix} G_{:z} & G_{:u_1} & \dots & G_{:u_i} & \dots & G_{:u_N} \end{bmatrix} \begin{bmatrix} 0_{n_z \times n_p} & 0_{n_z \times 6} & \dots & 0_{n_z \times 6} & \dots & 0_{n_z \times 6} \\ 0_{6 \times n_p} & 0_{6 \times 6} & \dots & 0_{6 \times 6} & \dots & 0_{6 \times 6} \\ \vdots & \vdots & \ddots & \vdots & \iddots & \vdots \\ 0_{6 \times n_p} & 0_{6 \times 6} & \dots & M & \dots & 0_{6 \times 6} \\ \vdots & \vdots & \iddots & \vdots & \ddots & \vdots \\ 0_{6 \times n_p} & 0_{6 \times 6} & \dots & 0_{6 \times 6} & \dots & 0_{6 \times 6} \end{bmatrix} \begin{bmatrix} G^i_{pz} \\ G^i_{y_1 z} \\ \vdots \\ G^i_{y_i z} \\ \vdots \\ G^i_{y_N z} \end{bmatrix} \tag{8}$$

$$G\boldsymbol{M}_i G^i_{:z} = G_{:u_i} M G^i_{y_i z}. \tag{9}$$

The resulting equation

$$G^i_{:z} - G_{:z} = G_{:u_i} M G^i_{y_i z} \tag{10}$$

is still formulated for system G which is not directly obtained from experiment. The outputs u_i can be determined from the actually measured outputs $\tilde{u}_i$ by e.g. the VPT. The next step is to substitute these quantities by their experimentally obtained counterparts. The required transformations are $G^i_{:z} = T_O \tilde{G}^i_{:z}$, $G_{:z} = T_O \tilde{G}_{:z}$, and $G^i_{y_i z} = T^i_O \tilde{G}^i_{\tilde{y}_i z}$, also see Equations (3) and (4), which results in

$$\begin{aligned} \underbrace{T_O \left[\tilde{G}^i_{:z} - \tilde{G}_{:z} \right]}_{\Delta G^i} &= G_{:u_i} & \underbrace{M T^i_O \tilde{G}^i_{\tilde{y}_i z}}_{G^i_M} \\ \Delta G^i &= G_{:u_i} & G^i_M \end{aligned} \tag{11}$$

where no input transformation is required for the reference inputs, and $\Delta G^i \in \mathbb{C}^{n_O \times n_z}$ and $G^i_M \in C^{6 \times n_z}$. Equation (11) can be solved for the required quantity $G_{:u_i}$. The standard non-parametric estimate of an FRF is defined on a frequency grid $\Omega = \{\omega_1, ..., \omega_{n_\omega}\}$. For such estimates, Equation (11) can be solved for each frequency separately. Explicitly including the frequency-dependency, the equation can be solved at $\omega_k \in \Omega$ by

$$G_{:u_i}(\omega_k) = \Delta G^i(\omega_k) G^{i+}_M(\omega_k) \tag{12}$$

where $G^{i+}_M(\omega_k)$ is the pseudo-inverse of G^i_M at frequency ω_k.

The main issue of this procedure is the number of unknowns. A necessary condition for an over-determined pseudo-inverse G^{i+}_M is that the number of reference inputs $n_z \geq 6$ as $G^i_M \in C^{6 \times n_z}$ which allows to calculate $G_{:u_i}(\omega_k)$ based on a minimal error. As one main benefit of AMPIE is supposed to be the limited number of excitation points and mounting operations, increasing n_z contrasts this benefit. Another way to counteract this issue is to repeat the procedure for different masses $M_j \in \{M_1, ..., M_{n_M}\}$ at driving point i, i.e. to use multiple masses. To distinguish the individual masses, the index $j \in \{1, ..., n_M\}$ is introduced. Without loss of generality, the number of masses n_M is chosen to be the same for all driving points to avoid unnecessary indices. Note that a different number of masses could be used in practice, but only complicates the notation. Consequently, the measurement procedure results in $G_{:z}$ and $G^{ij}_{:z}$ where the particular mass is addressed by the superscript j. Furthermore, the matrix $\boldsymbol{M}_i$ is also formulated

as

$$\boldsymbol{M}_{ij} = \begin{array}{c} \\ \\ \\ \\ \\ \\ \\ \end{array} \begin{array}{c} \begin{array}{ccccccc} & & & \text{Driving} & \text{Point} & \text{index:} & \\ & 1 & & \rightarrow & i & \rightarrow & N \end{array} \\ \begin{bmatrix} 0_{n_z \times n_p} & 0_{n_z \times 6} & \dots & 0_{n_z \times 6} & \dots & 0_{n_z \times 6} \\ 0_{6 \times n_p} & 0_{6 \times 6} & \dots & 0_{6 \times 6} & \dots & 0_{6 \times 6} \\ \vdots & \vdots & \ddots & \vdots & \iddots & \vdots \\ 0_{6 \times n_p} & 0_{6 \times 6} & \dots & M_j & \dots & 0_{6 \times 6} \\ \vdots & \vdots & \iddots & \vdots & \ddots & \vdots \\ 0_{6 \times n_p} & 0_{6 \times 6} & \dots & 0_{6 \times 6} & \dots & 0_{6 \times 6} \end{bmatrix} \end{array} \begin{array}{c} \\ 1 \\ \downarrow \\ i \\ \downarrow \\ N \end{array} \tag{13}$$

The application of multiple masses can be achieved directly based on Equation (11). Notice that $G_{:u_i}$ does not depend on the specific mass that is coupled. In contrast, the items ΔG^i and G_M^i change with different values of M_j and must be distinguished if multiple masses are used. This is also achieved by a second superscript j that accounts for M_j which leads to the adapted quantities from Equation (11):

$$\Delta G^{ij} = T_O \left[\tilde{G}_{:z}^{ij} - \tilde{G}_{:z} \right] \tag{14}$$

$$G_M^{ij} = M_j T_O^i \tilde{G}_{\tilde{y}_i z}^{ij}. \tag{15}$$

For all masses $M_j \in \{M_1, ..., M_{n_M}\}$, Equation (11) is obtained n_M times which results in

$$\left.\begin{array}{rcl} \Delta G^{i1} & = & G_{:u_i} G_M^{i1} \\ & \vdots & \\ \Delta G^{ij} & = & G_{:u_i} G_M^{ij} \\ & \vdots & \\ \Delta G^{in_M} & = & G_{:u_i} G_M^{in_M} \end{array}\right\} \Rightarrow \left[\Delta G^{i1} \quad ... \quad \Delta G^{ij} \quad ... \quad \Delta G^{in_M} \right] = G_{:u_i} \left[G_M^{i1} \quad ... \quad G_M^{ij} \quad ... \quad G_M^{in_M} \right].$$

The resulting equation to obtain $G_{:u_i}$ is

$$G_{:u_i}(\omega_k) = \left[\Delta G^{i1}(\omega_k) \quad \dots \quad \Delta G^{in_M}(\omega_k) \right] \left[G_M^{i1}(\omega_k) \quad \dots \quad G_M^{in_M}(\omega_k) \right]^+. \tag{16}$$

where the pseudo-inverse condition is $n_z n_M \geq 6$. Still, as shown in Section 4 and C.2, this approach may not yield acceptable results.

Using multiple masses increases the available amount of data, which manifests in additional columns for the pseudo-inverse in Equation (16). A second possibility to improve the obtained results is to use parametric, linear systems which reduces the total number of unknowns. For the studied example, this combination of multiple masses and parametric systems was required to obtain acceptable results. Therefore, the application of parametric, linear systems in the present scheme is subsequently described.

2.3 Application of Parametric Systems

Based on system identification [29, 30, 31] in the field of system and control theory or modal analysis [32, 33] in the field of structural dynamics, parametric systems can be obtained from measurement data. In substructuring, the application of parametric state-spaces systems was mainly driven by Sjövall, Gibanica, and Abrahamsson, for example in [34, 35]. The FRF of a parametric, linear state-space system with acceleration outputs is given by $G(\omega) = C(\boldsymbol{i}\omega I - A)^{-1} B + D$ [28], where $A \in \mathbb{R}^{n \times n}$ is the state, $B \in \mathbb{R}^{n \times n_I}$ is the input, $C \in \mathbb{R}^{n_O \times n}$ is the output, and $D \in \mathbb{R}^{n_O \times n_I}$ is the feedthrough matrix. For a mechanical system, the state-matrix A can be associated with eigenfrequencies and their corresponding damping, the input- and output-matrix B and C can be associated with mode-shapes, whereas the feedthrough D depends on the chosen outputs. In addition to a given number of outputs and inputs, a user-defined number of n states is required for such models. The state can be transformed arbitrarily and is chosen such that all matrices are real-valued. The bold symbol $\boldsymbol{i}$ denotes the imaginary part, in contrast to the index i that addresses particular driving points. Since the system describes a mechanical structure that is in theory

described by a second order model [36, p. 153, 480], the equation $D = CA^{-1}B$ can be put forward for the feedthrough matrix, resulting in

$$G = C(\boldsymbol{i}\omega I - A)^{-1}B + CA^{-1}B = C\left[(\boldsymbol{i}\omega I - A)^{-1} + A^{-1}\right]B = C\Lambda(\omega)B \tag{17}$$

where $\Lambda(\omega) = \left[(\boldsymbol{i}\omega I - A)^{-1} + A^{-1}\right] \in \mathbb{C}^{n\times n}$ accounts for frequency-dependencies and the matrices B and C are constant. The constraint $D = CA^{-1}B$ is not fulfilled by default and must, therefore, be enforced after the identification. One way to enforce the constraint is discussed in Appendix D. It is important to notice, that the identification procedure of the parametric system requires additional effort. Note that the partitioning from Equation (2) is achieved column-wise by separating the matrix B according to

$$G = \begin{bmatrix} G_{:z} & G_{:u_1} & \dots & G_{:u_N} \end{bmatrix} = C\Lambda(\omega)\begin{bmatrix} B_{:z} & B_{:u_1} & \dots & B_{:u_N} \end{bmatrix} \tag{18}$$

$$\Rightarrow G_{:z} = C\Lambda(\omega)B_{:z}, \quad B_{:z} \in \mathbb{R}^{n\times n_z} \tag{19}$$

$$\Rightarrow G_{:u_i} = C\Lambda(\omega)B_{:u_i}, \quad B_{:u_i} \in \mathbb{R}^{n\times 6}. \tag{20}$$

The separation makes clear that in case of the AMPIE scheme, the parametric system which is fitted to the measured data is $G_{:z} = C\Lambda(\omega)B_{:z}$. Similar to the FRF-based approach, the missing inputs at driving point i are expressed by $G_{:u_i} = C\Lambda(\omega)B_{:u_i}$, where the remaining unknown quantity is $B_{:u_i}$. Before the solution process for $B_{:u_i}$ is described, it is worth to take a closer look at the involved quantities and their implications.

The basis for the estimation of $B_{:u_i}$ via the AMPIE strategy is $G_{:z} = C\Lambda(\omega)B_{:z}$. This identified system $G_{:z} = C\Lambda(\omega)B_{:z}$ offers a modal basis solely by the excitation of z. When z is excited, dynamics at the coupling points are only detected by the outputs $y_1, ..., y_N$ as $u_1, ..., u_N$ is not excited during the measurement of $G_{:z}$ and throughout the entire AMPIE procedure. Concluding, in the presented form, the approach requires that all eigenmodes that are excited by an excitation at u_i are also excited by z. Otherwise, the coupling of a mass at driving point i would excite dynamics, that cannot be described by $G_{:z} = C\Lambda(\omega)B_{:z}$. Note that this limitation is also present in the FRF-based formulation but does not emerge this clearly.

Assuming that all dynamics can be described by the identified system, for driving point i and mass j, Equation (11) becomes

$$\Delta G^{ij}(\omega) = G_{:u_i}G_M^{ij}(\omega) = C\Lambda(\omega)B_{:u_i}G_M^{ij}(\omega). \tag{21}$$

The decisive difference between Equation (21) and Equation (11) is that the unknown quantity $B_{:u_i}$ is a frequency-*independent* matrix. This changes the mathematical foregoing to solve the equation for $B_{:u_i}$. It is worth noting that this problem is mathematically similar to several joint identification approaches, e.g. proposed by Ren and Beards [37].

In order to obtain the unknown quantity $B_{:u_i}$, the equation can be manipulated using the Kronecker-product. The unknown quantity X in the matrix-valued equation $AXB = C$ can be obtained from the Linear Equation System (LES) $(B^{\mathsf{T}} \otimes A)\downarrow X = \downarrow C$ where $\downarrow$ denotes the column-wise vectorization of a matrix, i.e. $\downarrow\begin{bmatrix} x_1 & \dots & x_n \end{bmatrix} = \begin{bmatrix} x_1^{\mathsf{T}} & \dots & x_n^{\mathsf{T}} \end{bmatrix}^{\mathsf{T}}$ and $\otimes$ is the Kronecker-product. For mass j at driving point i, the obtained equation is a complex-valued, linear equation system with a frequency-independent, real-valued unknown x, allowing the separation of real and imaginary parts

$$\underbrace{\downarrow\Delta G^{ij}(\omega)}_{b_{ij}(\omega)} = \underbrace{[G_M^{ij,\mathsf{T}}(\omega) \otimes C\Lambda(\omega)]}_{A_{ij}(\omega)}\underbrace{\downarrow B_{:u_i}}_{x_i} \rightarrow \begin{bmatrix} A_{ij}^R(\omega) \\ A_{ij}^I(\omega) \end{bmatrix} x_i = \begin{bmatrix} b_{ij}^R(\omega) \\ b_{ij}^I(\omega) \end{bmatrix}, \tag{22}$$

where $x_i \in \mathbb{R}^{6n\times 1}$ is the real-valued unknown quantity, and the complex-valued quantities $b_{ij}(\omega) \in \mathbb{C}^{n_O n_z\times 1}$ and $A_{ij}(\omega) \in \mathbb{C}^{n_O n_z\times 6n}$ are separated into their real and imaginary parts $b_{ij}^R(\omega) \in \mathbb{R}^{n_O n_z\times 1}$, $b_{ij}^I(\omega) \in \mathbb{R}^{n_O n_z\times 1}$, $A_{ij}^R(\omega) \in \mathbb{R}^{n_O n_z\times 6n}$, and $A_{ij}^I(\omega) \in \mathbb{R}^{n_O n_z\times 6n}$ to form a real-valued LES. Except for x_i, the quantities in this equation are frequency-dependent. However, apart from $\Lambda(\omega)$, the quantities are not assumed to be available in a frequency-continuous but a frequency-discrete from, i.e. on a frequency grid $\omega_k \in \Omega = \{\omega_1, ..., \omega_{n_\omega}\}$, such as the typical, non-parametric estimate of a frequency-response function. Multiple frequencies are included in Equation (22) by stacking the quantities accordingly:

$$\begin{bmatrix} A_{ij}^R(\omega_1) \\ A_{ij}^I(\omega_1) \\ \vdots \\ A_{ij}^R(\omega_{n_\omega}) \\ A_{ij}^I(\omega_{n_\omega}) \end{bmatrix} x_i = \begin{bmatrix} b_{ij}^R(\omega_1) \\ b_{ij}^I(\omega_1) \\ \vdots \\ b_{ij}^R(\omega_{n_\omega}) \\ b_{ij}^I(\omega_{n_\omega}) \end{bmatrix} \Rightarrow A_{ij}^{RI} x_i = b_{ij}^{RI}. \tag{23}$$

The number of used frequencies leads to $A_{ij}^{RI} \in \mathbb{R}^{2n_\omega n_O n_z \times 6n}$ and $b_{ij}^{RI} \in \mathbb{R}^{2n_\omega n_O n_z \times 1}$ where the number of unknowns $6n$ is typically smaller than the number of equations $2n_\omega n_O n_z$. This can be approached by a minimization of the least-squares error which results in a quadratic equation system $(A^\mathsf{T} W A)x = A^\mathsf{T} W b$ with a weighting matrix W. Formulated for the present case, the weighting is defined frequency-wise. Therefore, the equation can be re-formulated as sum

$$A_{ij}^{\blacksquare} x_i = b_{ij}^{\blacksquare} \quad \text{with:} \tag{24}$$

$$A_{ij}^{\blacksquare} = \sum_{k=1}^{n_\omega} \underbrace{A_{ij}^{R,\mathsf{T}}(\omega_k) W_k^R A_{ij}^R(\omega_k) + A_{ij}^{I,\mathsf{T}}(\omega_k) W_k^I A_{ij}^I(\omega_k)}_{\Delta A_{ij}^{\blacksquare}(\omega_k)} \tag{25}$$

$$b_{ij}^{\blacksquare} = \sum_{k=1}^{n_\omega} \underbrace{A_{ij}^{R,\mathsf{T}}(\omega_k) W_k^R b_{ij}^R(\omega_k) + A_{ij}^{I,\mathsf{T}}(\omega_k) W_k^I b_{ij}^I(\omega_k)}_{\Delta b_{ij}^{\blacksquare}(\omega_k)} \tag{26}$$

where $A_{ij}^{\blacksquare} \in \mathbb{R}^{6n \times 6n}$, $b_{ij}^{\blacksquare} \in \mathbb{R}^{6n \times 1}$. The matrices $W_k^R \in \mathbb{R}^{n_O n_z \times n_O n_z}$ and $W_k^I \in \mathbb{R}^{n_O n_z \times n_O n_z}$ are weighting matrices at frequency ω_k, defined for the real and imaginary quantities separately. As FRFs typically span several orders of magnitude, this is also true for the values in the sums (25) and (26). The application in the scope of this work shows that a relative weighting $W_k^R = \text{diag}(b_{ij}^R(\omega_k))^{-1}$ and $W_k^I = \text{diag}(b_{ij}^I(\omega_k))^{-1}$ is beneficial.

Similar to the previous NP-FRF-based discussion, the application of more than one mass is beneficial. As for Equation (23), where all frequencies are stacked, n_M masses are included by further stacking, which ultimately results in further summation:

$$\begin{bmatrix} A_{i1}^{RI} \\ \vdots \\ A_{in_M}^{RI} \end{bmatrix} x_i = \begin{bmatrix} b_{i1}^{RI} \\ \vdots \\ b_{in_M}^{RI} \end{bmatrix} \Rightarrow A_i^{\blacksquare} = \sum_{j=1}^{n_M} A_{ij}^{\blacksquare}, \; b_i^{\blacksquare} = \sum_{j=1}^{n_M} b_{ij}^{\blacksquare}. \tag{27}$$

The quantity $B_{:u_i}$ is then obtained by reshaping x_i that is the solution of the LES

$$A_i^{\blacksquare} x_i = b_i^{\blacksquare} \Rightarrow x_i = (A_i^{\blacksquare})^{-1} b_i^{\blacksquare}. \tag{28}$$

2.4 Summary, Comparison, and Practical Considerations

Summary At first, the main steps that were outlined in the previous section are briefly summarized:

- The overall goal is to obtain a system G that is suited for substructuring by offering 6-by-6 driving points for coupling other systems.
- In a standard measurement scenario, the system $\tilde{G}$ is obtained, where the main experimental effort is found to obtain the submatrices $G_{:u_i} = T_O \tilde{G}_{:\tilde{u}_i}$ which are frequently obtained by using adapter structures.
- The dynamic modification of the structure resulting from an added mass, similar to an adapter structure, is exploited in the AMPIE strategy, where the matrices $G_{:z} = T_O \tilde{G}_{:z}$ without mass and $G_{:z}^{ij} = T_O \tilde{G}_{:z}^{i}$ with mass j at driving point i are used as input to obtain $G_{:u_i}$ based on the observed difference.
- The basis for the derivation is to formulate the effect of the coupled mass as constant feedback in Equation (5). The difference in the solution process between AMPIE and MUM are pointed out in Appendix B.
- The NP-FRF-based derivation to obtain $G_{:u_i}$ ultimately leads to a LES (11) that can be solved by a pseudo-inverse, which is formulated for a single mass in Equation (12) and for multiple masses in Equation (16).

- Based on the LES (11) and the FRF of a parametric state-space system $G(\omega) = C\Lambda(\omega)B$ the problem can be reformulated in calculating the frequency-independent matrix $B_{:u_i}$ from Equation (28) instead of the frequency-dependent quantity $G_{:u_i}$. The required constraint and its application to the state-space system is discussed in Appendix D.

Furthermore, the procedure can conveniently be denoted as algorithm, see Appendix A. For a scenario with

- n_O outputs, and n_z reference inputs,
- N driving points, a constant number of n_M masses per coupling point,
- a parametric system with n states,
- that is evaluated on n_ω frequencies,

the AMPIE scheme is given in Procedure 1 for the measurements, as well as Procedure 2 and Procedure 3 for the non-parametric and parametric data-processing, respectively. Note that the number of masses could vary, but is chosen to be constant for a clear notation. In addition to the algorithmic summary, the comparison of the parametric versus the non-parametric approach are addressed subsequently.

Parametric and Non-Parametric The strategies are compared using pseudo-code in Procedure 2 and 3. Apart from the procedures, the ratio ρ of the number of unknowns and available equations is of interest as $\rho > 1$ is a necessary condition that the LES from Equation (16) or Equation (28) can be solved uniquely which was already discussed for Equation (16). This ratio is listed in Table 1:

Procedure	Unknowns	Equations	Ratio ρ
Non-Parametric (16)	$2 \cdot 6 \cdot n_O$	$2 \cdot n_O n_z n_M$	$\frac{n_z n_M}{6}$
Parametric (28)	$6n$	$2n_O n_z n_M n_\omega$	$\frac{n_O n_z n_M n_\omega}{3n}$

Table 1: Overview of equations, unknowns, and ratio ρ.

The number of equations for the parametric case is increased based on two effects. First, the required quantity is real-valued, which is not the case for the non-parametric calculation. Real and imaginary part can be split into two sets of equations, adding the factor 2. That same factor is found in the non-parametric case for equations and unknowns, leading to its cancellation. Second, all frequencies are used for the parametric approach, adding the coefficient n_ω. However, for the parametric case, the number of states n determines the number of unknowns. This highlights the importance of the used, identified system. Accuracy and number of states have a decisive influence and must be carefully traded off in the identification process. A concept for assessing the AMPIE procedure based on predictions and test-cases is introduced subsequently.

Prediction and Test-Case The outlined approach is based on the minimization of the least-squares errors in Equation (12), for the NP-FRF-based approach, and Equation (23) for the state-space-based approach. It is clear that this error will be smaller, the more variables are available. Due to this overfitting effect, the minimized least-squares error is not suited to measure the quality of the obtained quantities. Instead, the initially stated feedback from Equation (5) can be used. An entire overview of the subsequently discussed concepts is given in Figure 5.

The results of the described procedure is $G_{:u_i}$. Therefore, the coupling operation (5) can be computed based on the now known system $G = \begin{bmatrix} G_{:z} & G_{:u_1} & \dots & G_{:u_N} \end{bmatrix}$, resulting in a prediction for the system with coupled mass $\boldsymbol{M}_{ij}$ from Equation (13)

$$G^{ij,\star} = (I - G\boldsymbol{M}_{ij})^{-1} G. \tag{29}$$

The resulting submatrix $G^{ij,\star}_{:z}$ can be compared to the values $G^{ij}_{:z} = T_O \tilde{G}^{ij}_{:z}$ that were experimentally obtained. It is important to notice, that the obtained prediction-error $G^{ij,\star}_{:z} - G^{ij}_{:z}$ and the least-square error in Equation (12) or (23) are vastly different. For example, increasing the number of states n would continuously reduce the least-square error, but would at some point start to increase the deviation in the obtained predictions $G^{ij,\star}$. Further, it is important to notice that the concept to predict the quantity $G^{ij,\star}$ does not depend on whether the information G^{ij} was used in the

estimation process, i.e. in Equation (12) or Equation (23). This observation and the need to validate the obtained quantities leads to the concept of a test-case.

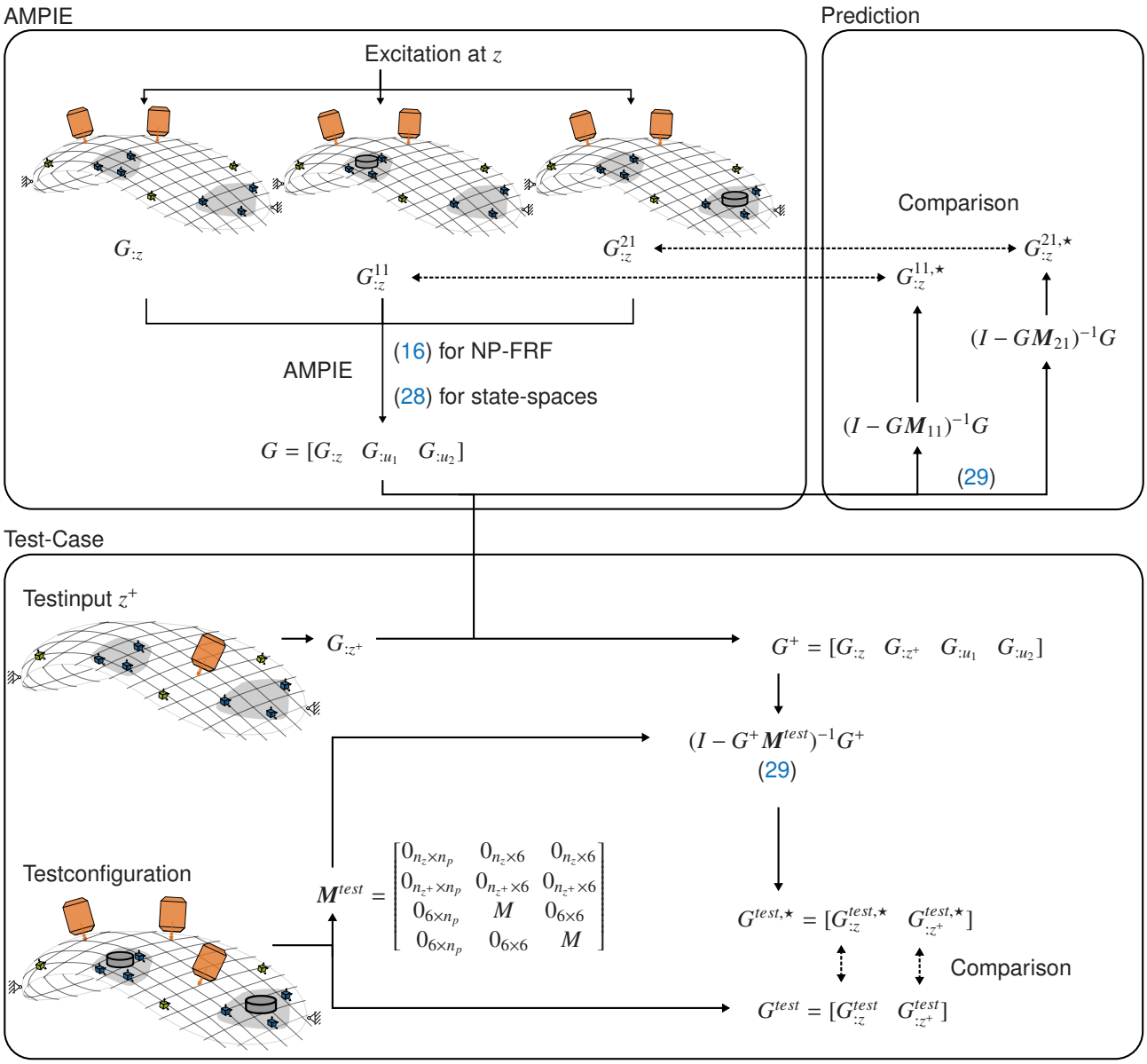

Fig. 5: Generic example illustrating the relation between AMPIE, predictions and test-cases.

In order to obtain the required input quantities, a set of reference inputs was combined with a set of masses. The resulting quantities $G_{:z}^{ij}$ were used in the estimation of $G_{:u_i}$. In order to validate the obtained results further, beyond the concept of predictions $G_{:z}^{ij,\star}$, a test-case is constructed that includes further unknowns. There are two possible ingredients for such a test-case. First, the attachment of arbitrary mass or substructure configurations can be tested. Here, the main question is, if the obtained results are only suited to reproduce the input data, i.e. the coupling of one mass at one position, or more complex scenarios as well, for example two masses which are attached simultaneously at two positions. Second, the test can involve reference inputs $z^+ \in \mathbb{C}^{n_{z^+} \times 1}$ that were not included in the computation procedure. The motivation for the latter case is straightforward: Procedure 1 makes clear, that the experimental effort rises with the number of reference inputs n_z that are included in the AMPIE procedure. The idea of a test-case is, that the quantities $G_{:z}$ and $G_{:z^+} \in \mathbb{C}^{n_O \times n_{z^+}}$ as well as all $G_{:z}^{ij}$ are recorded whereas the quantities $G_{:z^+}^{ij}$ are not recorded. For the AMPIE procedure, only $G_{:z}$ and $G_{:z}^{ij}$ are used to estimate $\begin{bmatrix} G_{:u_1} & \dots & G_{:u_N} \end{bmatrix}$ via Equation (16) or Equation (28). Then, the entire system $G^+ = \begin{bmatrix} G_{:z} & G_{:z^+} & G_{:u_1} & \dots & G_{:u_N} \end{bmatrix} \in \mathbb{C}^{n_O \times (n_I + n_{z^+})}$ is used in Equation (29) which results in

$G^{test,\star} = \begin{bmatrix} G^{test,\star}_{:z} & G^{test,\star}_{:z^+} \end{bmatrix}$. This prediction is then compared to $G^{test} = \begin{bmatrix} G^{test}_{:z} & G^{test}_{:z^+} \end{bmatrix}$ which is the measured reference for the arbitrary configuration of coupled substructures with additional reference inputs z^+. An example is given in Figure 5.

Figure 5 summarizes the discussed concepts – AMPIE, prediction, and test-case – using the generic example that was already used in the introduction. For the illustrated AMPIE procedure, the only difference to Figure 4 is the formulation of the involved quantities with superscript j. Note that the example is not extended to multiple masses to avoid an overloaded illustration. In addition, the main equations are given which result in the system G. Based on this system, the concept of a prediction is shown in the upper right part of Figure 5. The feedback equation is solved for $\boldsymbol{M}_{11}$ and $\boldsymbol{M}_{21}$. The concept for a test-case is illustrated in the lower part of the figure. It makes clear that $G_{:z^+}$ must be measured and is inserted in G to form G^+. The illustrated test-configuration is defined by two masses, which result in the matrix $\boldsymbol{M}^{test}$ for Equation (29) and ultimately in $G^{test,\star}$ which is compared to the experimentally obtained quantities G^{test}.

3 Experimental Example

Figure 6 shows the scenario that is used to analyze the outlined scheme. The specimen consists of a welded steel frame with bolt-on steel and acrylic glass plates. The measurement set-up is defined by six reference outputs and three reference inputs. Two of these inputs are used to generate the input data for the AMPIE procedure, i.e. $z = \begin{bmatrix} z_1 & z_2 \end{bmatrix}$, the third is used within the test-case, i.e. $z^+ = z_3$ which was explained in detail in Figure 5. Two coupling points are analyzed. To establish a virtual point transformation for the measured output accelerations, three triax accelerometers are mounted at each coupling point. This results in $\tilde{y}_1$ and $\tilde{y}_2$ for the first and second coupling point, respectively. Two additional triax accelerometers are placed at different locations and represent the reference outputs $p_1 - p_6$. In summary, the recorded systems have two input and 24 output signals. The entire system is fixed in the middle of the lower part of the frame, the support is symbolized by hatched lines.

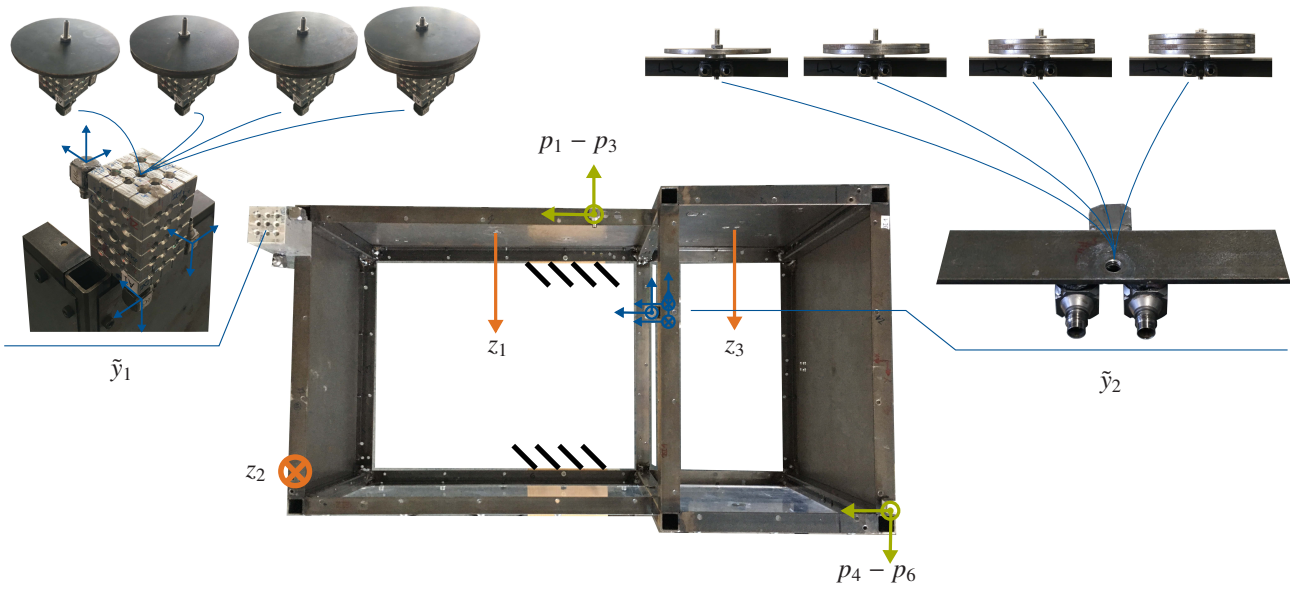

Fig. 6: Channel set-up for the analysis of the AMPIE approach and used added masses.

On both coupling points, a total of four masses is attached successively which results in $G^{ij}_{:z}$. The mass is increased by stacking equivalent discs. This set-up has two advantages: first, the mounting operation is straightforward and can be tracked and documented easily, and, second, the incremental definition based on the index j allows a convenient implementation in the subsequent analysis. The VPT is defined such that the acceleration outputs on both coupling points are transformed to a local coordinate system, that corresponds to Figure 7. Both, the aluminum block of driving point 1 and the area of driving point 2 that is defined by the three accelerometers in approximately 20mm radius, are considered to be sufficiently stiff to allow a VPT in the frequency range to 200Hz. The resulting values for M_j can be obtained from Equation (30).

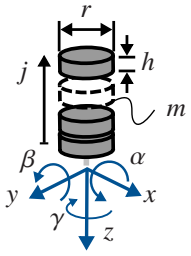

$$M_j = \begin{bmatrix} m & 0 & 0 & 0 & -\frac{\bar{m}\bar{h}}{2} & 0 \\ 0 & m & 0 & \frac{\bar{m}\bar{h}}{2} & 0 & 0 \\ 0 & 0 & m & 0 & 0 & 0 \\ 0 & \frac{\bar{m}\bar{h}}{2} & 0 & J_{\alpha\alpha} & 0 & 0 \\ -\frac{\bar{m}\bar{h}}{2} & 0 & 0 & 0 & J_{\beta\beta} & 0 \\ 0 & 0 & 0 & 0 & 0 & J_{\gamma\gamma} \end{bmatrix} \text{ with: } \begin{cases} \bar{h} = jh, \bar{m} = jm \\ J_{\alpha\alpha} = J_{\beta\beta} = J_0 + J_s \\ J_0 = \frac{1}{4}\bar{m}(r^2 + \frac{1}{3}\bar{h}^2) \\ J_s = \bar{m}(0.5\bar{h})^2 \\ J_{\gamma\gamma} = 0.5\bar{m}r^2 \end{cases} \tag{30}$$

Fig. 7: Disc increments.

The total mass is defined by $\bar{m} = jm$, the total height of the resulting cylinder by $\bar{h} = jh$. As the coordinate system matches the rotational axes of the resulting cylinder, the obtained moment of inertia is diagonal. The visualization in Figure 7 and formula in Equation (30) show in detail, that the attached mass gives a force-feedback for translations and rotations which is used by the AMPIE strategy to determine the three input forces and three input torques in $G_{:u_i}$. The incremental definition (30) can be conveniently used in the implementation, see Procedure 2 and Procedure 3.

4 Results

In this section, results obtained from the proposed methods are discussed. First, the methods and algorithms used for system identification and AMPIE input data are summarized. Second, the results of the AMPIE procedure are investigated. Third, a test-case is outlined and evaluated.

System Identification and AMPIE Input All system identification steps for this publication were performed in MATLAB based on raw time-data that was recorded a sample rate of 2048Hz. The recorded outputs are accelerations, the recorded inputs are forces exerted by a shaker device. For the excitation band-limited noise was used. Consequently, all FRFs of analyzed reference channels G_{pz} have the units $\frac{m/s^2}{N}$. Channels associated with coupling have different units associated with translations and rotations, e.g. $\frac{m/s^2}{Nm}$, $\frac{rad/s^2}{N}$, or $\frac{rad/s^2}{Nm}$. However, as described in the introduction in Section 2.1, the assessment focuses on the reference channels.

The parametric system identification for $G_{:z}$ which is required to enable the state-space-based procedure outlined in Section 2.3 was conducted using the $\mathrm{N4SID}$ routine with the CVA-method [38] that is offered in the MATLAB System Identification Toolbox [39]. The constraint $D = CA^{-1}B$ is enforced subsequently, as described in Appendix D. The identified model consists of 150 states, which were manually chosen by comparing the parametric FRF with the non-parametric one, and is found to accurately describe the frequency range from 10 to 200Hz. The assessment of the accuracy is based on the visual comparison of the FRFs, for example on the channels shown in Figure 8. One finds, that there is no significant deviation between the FRFs. Several out-of-band modes are required to accurately describe the frequency range. Compared to the NP-FRF $G_{:z}$, the identified model will be more accurate, the more states are used. However, as discussed earlier, an arbitrary high number of states is not recommended as the increased number of variables will eventually deteriorate the obtained results from the AMPIE procedure. The channels $[p_6] \leftarrow [z_1, z_2, z_3]$ from the NP-FRF $G_{:z}$, and state-space $G_{:z}$ with and without constraint are shown in Figure 8. The arrow-notation is used to highlight that the FRF describes the effect of the set of inputs on the outputs. The arrow points to the left in accordance with the standard notation of the underlying matrix multiplication. Compared to an index-based notation, e.g. G_{pz}, the arrow-notation offers the advantage that channels can be addressed without specifying a system. This is exploited in the layout of the subsequently discussed plots where the channels are specified in the caption using the arrow notation. The systems are specified in the legend, which makes the Figures clearer.

All non-parametric FRF were estimated using the SPAFDR routine from the MATLAB System Identification Toolbox [39] which uses the Blackman-Tukey algorithm [40] based on a given frequency grid Ω. In this contribution, two different resolutions were used:

- Steps of 0.1Hz are used for all NP-FRFs in the AMPIE algorithm, i.e. $G_{:z}^{ij} \forall i \in 1, ..., N, j \in 1, ..., n_M$, and for the evaluation of the term $G_{:z} = C\Lambda(\omega)B_z$,
- Steps of 1Hz are used for all NP-FRFs associated with the test-case in G^{test}.

This difference is also clearly visible in the subsequently discussed graphs. A higher frequency resolution, increases the variance and noise in the graphs — particular at low amplitudes — as the used Hann windows are narrowed. The main idea behind the finer resolution in one set of NP-FRFs is the increased number of equations in the parametric AMPIE procedure, as shown in Table 1, Equation (27) and Section 2.4.

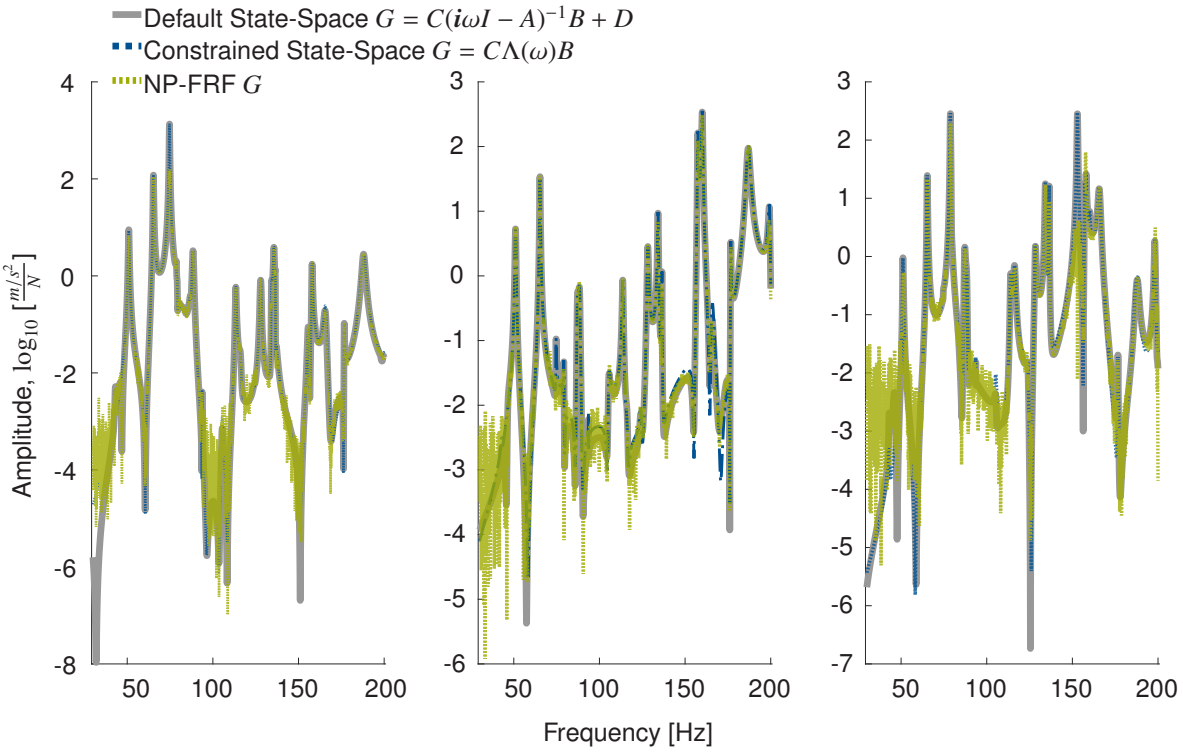

Fig. 8: AMPIE systems: default and constrained state-space systems that are used in the AMPIE procedure, along with the NP-FRF for comparison. The channels $[p_6] \leftarrow [z_1, z_2, z_3]$ from test set-up 6 are visualized.

Figure 8 clearly shows, that the FRF of the default and constrained state-space system match. Therefore, enforcing the constraint according to Appendix D, does not alter the identified state-space system in an undesired way. Both FRF also match with their non-parametric counterpart, no significant deviation can be detected.

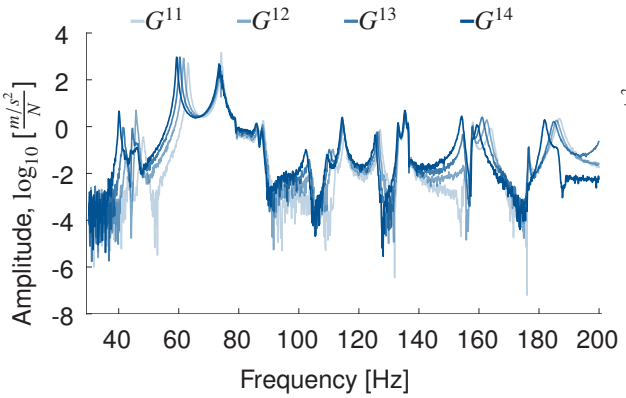

Fig. 9: Non-parametric AMPIE input data: shows the effect of an increasing mass coupled on position 1 for channel $[p_6] \leftarrow [z_1]$ from the test set-up in Figure 6.

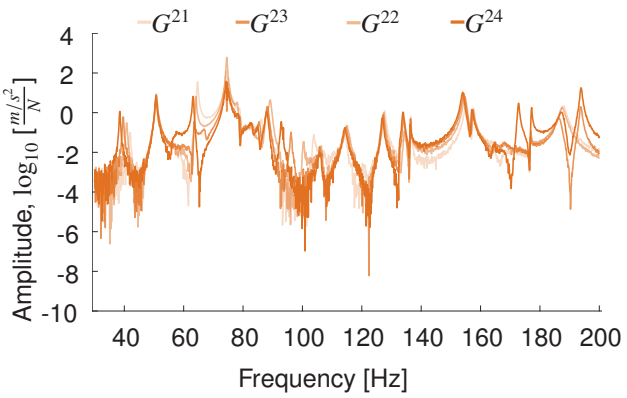

Fig. 10: Non-parametric AMPIE input data: shows the effect of an increasing mass coupled on position 2 for channel $[p_6] \leftarrow [z_1]$ from the test set-up in Figure 6.

Besides the system G, the specimen must be analyzed with attached masses. As illustrated in Figure 6, four masses are used at each coupling point, resulting in the systems $G_{:z}^{11} - G_{:z}^{14}$ and $G_{:z}^{21} - G_{:z}^{24}$. The channel $[p_6] \leftarrow [z_1]$ is plotted in Figure 9 for $G_{:z}^{11} - G_{:z}^{14}$ and in Figure 10 for $G_{:z}^{21} - G_{:z}^{24}$ where increasing opacity indicates a higher mass.

In most parts, the NP-FRFs plotted in Figure 9 and 10 meet the expectation: the transition between the incrementally altered systems is smooth and a gradual shift can be observed. However, there are regions that would intuitively be classified as outliers, for example $G_{:z}^{14}$ above 180Hz or $G_{:z}^{24}$ at 60Hz. This points to a decisive issue in the outlined schemes: the imperfection of recorded data due to random and systematic errors. The idea to use multiple masses is a first step to lower the sensitivity to deviations in single measurement results, however, the observation also suggest that systematic deviations become more likely, the higher the attached mass is, as the most significant outliers are present in $G_{:z}^{14}$ and $G_{:z}^{24}$, i.e. when four masses are coupled. There are several possible sources that can explain the systematic outliers, e.g.

- non-linear behavior that is gradually introduced by higher forces and torques, and thus higher displacements and rotations,
- static pretension that is not captured by the underlying system representation that only considers inert mass, not heavy mass,
- a higher likelihood for internal dynamics and in a larger stack of the attached discs,
- and their combination.

The precise analysis of the underlying physical mechanism is beyond the scope of this contribution. Rather, the list of different possible sources is intended to come to the important conclusion that methods that treat such systematic deviations and reduce their impact must be investigated further. Some ideas to approach this issue are discussed in Section 5.

AMPIE Results Given the systems $G_{:z}$, $G_{:z}^{11}$, ..., $G_{:z}^{14}$ and $G_{:z}^{21}$, .., $G_{:z}^{24}$, the Procedures 2 and 3 can be conducted. In case of the state-space-based Procedure 3, the resolution of the frequency grid was set to 0.1Hz. As discussed earlier, Equation (29) and the resulting system $\begin{bmatrix} G_{:z} & G_{:u_1} & G_{:u_2} \end{bmatrix}$ can be used to compute the predictions $G_{:z}^{11,\star}$, ..., $G_{:z}^{14,\star}$ and $G_{:z}^{21,\star}$, ..., $G_{:z}^{24,\star}$. The comparison to the input quantities $G_{:z}^{11}$, ..., $G_{:z}^{14}$ and $G_{:z}^{21}$, ..., $G_{:z}^{24}$ gives a first indication of the achieved accuracy. For the present scenario, the channel $[p_6] \leftarrow [z_1]$ from $G_{:z}^{13}$ and $G_{:z}^{13,\star}$, as well as $G_{:z}^{22}$ and $G_{:z}^{22,\star}$, are compared in Figure 11 and Figure 12, respectively. Note that this comparison only includes the state-space-based results.

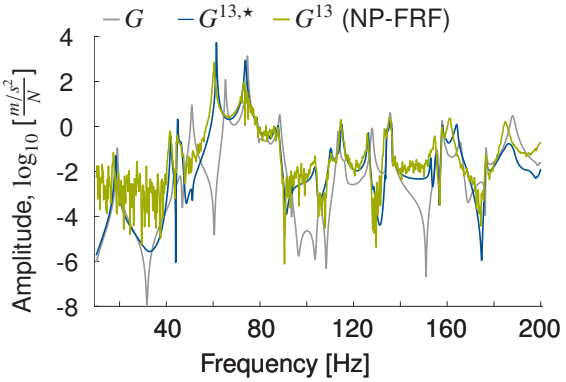

Fig. 11: AMPIE prediction for channel $[p_6] \leftarrow [z_1]$: measured and predicted result when three discs are coupled at position 1.

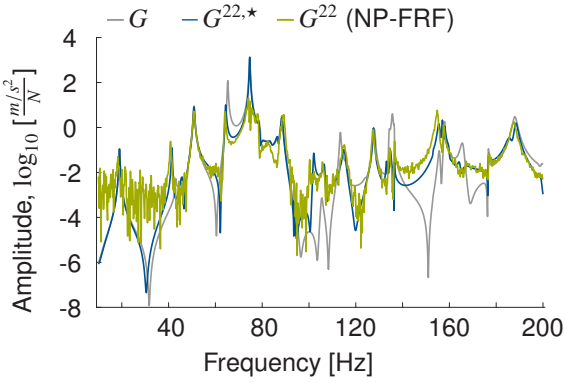

Fig. 12: AMPIE prediction for channel $[p_6] \leftarrow [z_1]$: measured and predicted result when two discs are coupled at position 2.

In summary, the predictions show a reasonable, but not a perfect reproduction of the measured data. For $G_{:z}^{13,\star}$, a mismatch above 180Hz is clearly visible. In case of $G_{:z}^{22,\star}$, the results show deviations between 140 and 160Hz as well as above 180Hz. Still, Figures 11 and 12 also show that the input data is affected by noise, in particular in regions with low amplitude, e.g. below 40Hz. Similar to possible systematic deviations in Figure 9 and 10, this emphasizes the need to deal with errors of random and systematic nature.

In order to asses if the obtained results can be used for further predictions, test-cases were discussed in Section 2.4. The main goal is to extend the assessment beyond the input data that has already been used in the AMPIE procedure. For the present example, the combination of masses is used instead of a single mass. This test-case is

still close to the used input data, however, it is chosen intentionally to avoid any further sources of uncertainty that would be introduced by a more complicated test-configuration. In addition, $z^+ = z_3$ is added in order to assess the ability to predict the effects of the test-case on an additional reference channel. This test-case is illustrated in Figure 13. The difference between the input and test data is shown in Figure 14 for channel $[p_6] \leftarrow [z_1]$.

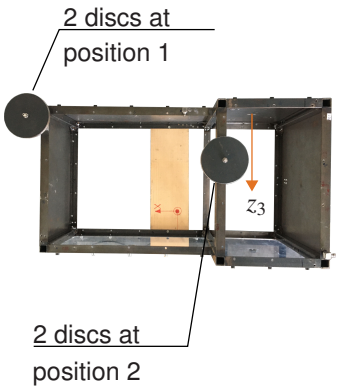

Fig. 13: Test-case: combination of masses at both positions and test-channel $z^+ = z_3$.

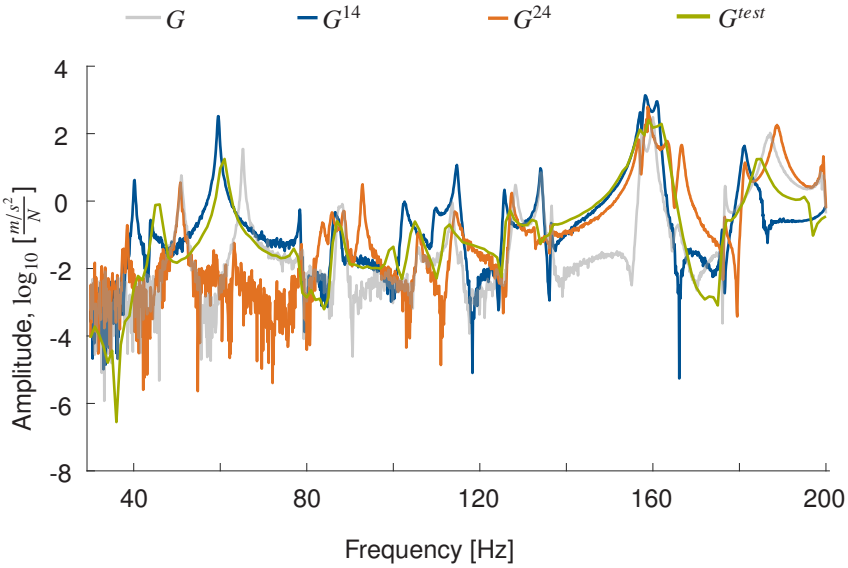

Fig. 14: Non-parametric AMPIE input and test-data for channel $[p_6] \leftarrow [z_1]$: the figure illustrates the difference between a mass combination G^{test} — realized by two discs simultaneously on both positions — and the used AMPIE data G^{14} and G^{24} obtained from coupling four discs on one of both positions as well es the default system G.

Figure 14 is used to show the difference between the default system, the AMPIE input data and the test-case. Since the test case is only based on attached masses, it is still close to the AMPIE input data. However, this figure is intended to show that the resulting dynamics are decisively different. This becomes particularly clear when the peaks of the FRFs are mutually compared. As an example, the low frequent-peaks of the default system G at approximately 50Hz and 65 Hz are briefly analyzed. In case of the system G^{14} the peaks are shifted to lower frequencies by approximately 10Hz. Instead, for G^{24} one peak vanishes, while the other is not significantly altered. For the two peaks the behavior of G^{test} is similar G^{14} as they are lowered by approximately 10Hz. A similar comparison can be put forward for several intervals of the shown FRF. In summary, the FRF of the test-case G^{test} show dynamics different from the default system, that cannot be attributed to the effect of one driving point. Therefore, it is considered as a suited test to assess if the estimated quantities of the AMPIE procedure can be used to predict the dynamics of such a combined configuration as the effect of both masses and their mutual influence must be incorporated.

The test prediction is shown in Figure 15 for channel $[p_2] \leftarrow [z_3]$, including the added reference input z_3. The same result is shown for channels $[p_2, p_6] \leftarrow [z_1, z_2, z_3]$ in Figure C.1. Similar to the prediction in Figures 11 and 12, the test-prediction $G^{test,\star}$ shows a reasonable match to the recorded reference G^{test}. In this case, reasonable means, that $G^{test,\star}$ comes close to G^{test}, in particular compared to the default system G which is the basis for the prediction according ot equation (29). Still, deviations similar to the above discussions can be observed. In the shown example, the accuracy significantly deteriorates above 180Hz, comparable to the case from Figure 11. Peaks that do not match the reference and may originate from overfitting can be observed, for example at roughly 75 and 160Hz. For the latter case at 160Hz, mismatches can also be found in Figure 11 and Figure 12. Besides the prediction that is obtained by using all 4 masses in Figure 15, Figure C.3 shows the results for one, two, and three masses as well. Using more masses clearly improves the results as one would expect. The outcome also underlines that, in the present example, at least one to three masses in the used configuration were required for usable results which emphasizes the possible benefits of the outlined approach.

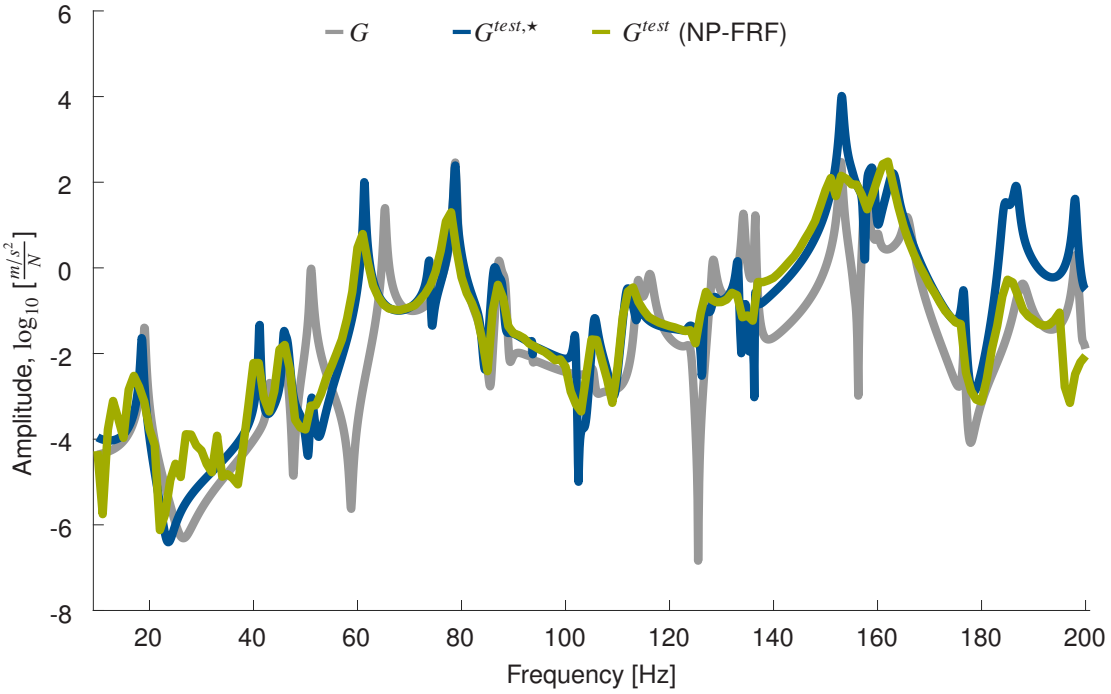

Fig. 15: AMPIE test-prediction for channel $[p_2] \leftarrow [z_3]$: default system as well as measured and predicted test-combination including the added test-channel z_3.

Example for Uncertainties Uncertainties were addressed in the paper, as they play an important role for an experiment-based approach like AMPIE. Some of the most relevant steps concerning uncertainty, e.g. quantification for parametric and non-parametric systems, the efficient propagation through the AMPIE calculations, approaches to counteract systematic and random deviations based on AMPIE-internal checks via Equation (29) and methods such as the Iterative Reweighted Least Squares (IRLS) [41, 42], require further research and an in-depth discussion on their own. This in-depth discussion is, to the authors' opinion, beyond the scope of this contribution. Rather than a comprehensive discussion of uncertainties, a limited example to provide an outlook on the effects of noise on the presented AMPIE strategy is given. The details of the chosen approach are briefly described. One limitation is, that uncertainties in the parametric system are not considered, i.e. for $G = C\Lambda(\omega)B_{:z}$ one sample is identified. For the remaining AMPIE inputs G^{ij}, 50 samples are generated for each system. The duration of the entire recorded data for each input z is 60 seconds. Samples are generated based on time frames with a duration of 10 seconds. In total 50 samples are generated for each system by shifting the sampled time frames by one second. Based on these samples, the AMPIE procedure is repeated 50 times. The resulting samples of $G^{test,\star}$ and the corresponding mean value are shown in Figure 16.

The main finding is, that the influence on uncertainties strongly depends on the frequency. For most parts of the analyzed frequency interval from 10 to 200 Hz, the samples are close to each other with little qualitative difference. In other words, considering one or the other sample would lead to a similar conclusion if the analyzed combination would be studied in order to tune the system G. For example, the peak at approximately 65Hz of system G is shifted to approximately 60Hz for the mean value of $G^{test,\star}$. Considering all samples, one finds that this shift is present in all samples within a 1Hz-interval which leads to the same qualitative conclusion in terms of the shifted frequency. In contrast, considering the amplitude of the shifted peak, the samples clearly show that its height can vary in a relevant interval. Concluding, in terms of amplitude, considering all samples leads to a different qualitative conclusion: the amplitude of the shifted peak can increase or decrease compared to the peak of G. If this height was of particular interest, the analyzed configuration would not be considered robust for system G. For other peaks, e.g. at approximately 105Hz, a different conclusion would be made. The discussed example, therefore, once more shows, that uncertainties are important to consider, albeit in a non-comprehensive approach.

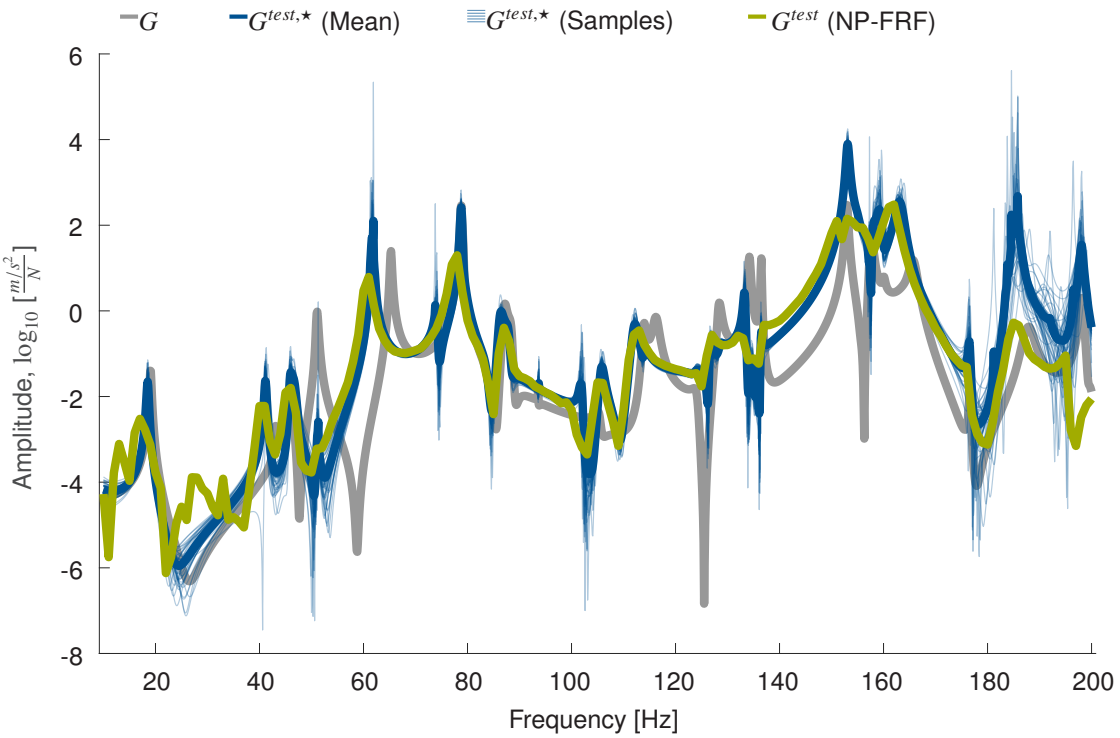

Fig. 16: AMPIE test-prediction for channel $[p_2] \leftarrow [z_3]$: default system as well as measured and predicted test-combination for the added test-channel z_3. for the predicted test-case $G^{test,\star}$, 50 samples are included.

The similarity of all samples cannot be confirmed for low amplitudes at anti-resonances, and for frequencies above 180Hz. The first finding can be expected as the noise to signal ratio is high at anti-resonances as the measured signals approach low values per definition at an anti-resonance. For the deviations above 180Hz, a possible explanation is the parametric system G. In order to accurately describe the frequency interval to 200Hz, out-of-band modes over 200Hz are required which do not represent physical behavior. Attaching masses can lower these peak which then introduce a higher uncertainty at the boundary of the studied frequency range of interest. Based on this reasoning, an important additional finding is, that a buffer interval should be included to avoid spurious effects in the frequency interval of interest.

In summary, these observations show that the outlined approach is capable to provide reasonable predictions beyond the used input data, while high attention must be payed to random and systematic deviations and imperfections in the input systems. This becomes particularly clear when results that are obtained from the NP-FRF-based Procedure 2 are included. For the present example, these results are shown in Figure C.2 for channels $[p_2, p_6] \leftarrow [z_1, z_2, z_3]$. It is clearly visible that the obtained prediction cannot be used. The noise in the input data is drastically amplified, yielding a completely perturbed result. Still, also a lower frequency resolution does not improve the significant bias. However, there are several further steps that can be used to tackle these issues, for parametric and non-parametric systems, which are part of further work on this strategy.

5 Summary, Conclusion and Further Work

Summary and Conclusion One of the main issues for substructuring is that driving points, in particular all 6-by-6 driving points, are hard to determine experimentally. Adapter structures are one of the most practical, purely experimental approaches, but require high mounting effort and numerical post-processing to eliminate the adapter's dynamics from the measurement. The idea that the effects of an attached structure, ideally a mass, on a specimen do not have to be eliminated but can be used to determine the input quantities of interest was introduced in the MUM [23, 11, 12], but mathematically limited to scalar input quantities and single masses. In this work, the AMPIE strategy is proposed, giving a straightforward notation and extending the basic idea from MUM to multiple masses, 6-by-6 driving points, and a formulation for parametric and non-parametric systems.

The assessment of the proposed schemes is based on the concept of predictions and test-cases. For the analyzed, simple test-case, promising results for the state-space-based approach can be obtained. Beyond the given input data, the effects of mass-combinations on an additional reference input can be predicted in most parts. However, deviations can clearly be detected. The main source for these deviations are random and systematic errors in the used data. As the AMPIE strategy can potentially reduce the measurement effort in certain scenarios, further work to tackle these issues is required.

Further Work The main source of error in the outlined schemes are random and systematic deviations in the input data. Therefore, the inclusion and treatment of these uncertainties beyond the given, non-comprehensive example is the most important next step. There are several possibilities to approach that issue.

First, the available experimental data can be used to quantify the uncertainty in the input systems. Based on such a representation, the uncertainty in the obtained results can be assessed. Further, based on the concept of the predicted quantities in Equation (29), optimization under uncertainty can be approached. Second, as Figure 9 and 10 show, the input data may lack consistency, that is expected due to the gradual increase of the attached mass. Automated approaches to exclude outliers are a further option. One possibility is the weighting. For example, Iterative Reweighted Least Squares (IRLS) [41, 42] can be an option in this context. Third, the proposed schemes allow to establish a 6-by-6 coupling point, however, not necessarily all entries are required in all cases or are free-to-choose. Constraints such as symmetry, or a diagonal shape may be enforced a priori, before the AMPIE procedure is conducted, resulting in a smaller set of unknowns. Fourth, a higher number of states yields a more accurate identified model, but will at some point deteriorate the estimation results. In further work, an automated selection of the number of states must be investigated.

Apart from extensions which further improve the used algorithm, additional experimental investigations are certainly required. In particular, the application to more complex substructuring scenarios is a key part of the further work. As this contribution shows the very basic capabilities and applicability of the proposed scheme, further investigations must include the comparison to the standard measurement procedure and compare them in terms of accuracy and experimental effort.

Appendix

A AMPIE Procedures

Procedure 1 AMPIE Measurements

Input: Measurement set-up
Output: $G_{:z}$ and $G_{:z}^{ij}$ $\forall i \in \{1, ..., N\}, j \in \{1, ..., n_M\}$

for $l \in \{1, ..., n_z\}$ ▷ iterate reference inputs
  Mount shaker at l, measure $G_{:z_l}$, append $G_{:z} \leftarrow G_{:z_l}$
  for $i \in \{1, ..., N\}$ ▷ iterate driving points
    for $j \in \{1, ..., n_M\}$ ▷ iterate added masses
      Add M_j at i, measure $G_{:z_l}^{ij}$, append $G_{:z}^{ij} \leftarrow G_{:z_l}^{ij}$
    end for
  end for
end for

Procedure 2 AMPIE Non-Parametric

Input: $G_{:z}$ and $G^{ij}_{:z} \forall i \in \{1, ..., N\}, j \in \{1, ..., n_M\}$
Output: G with $G_{:u_i} \forall i \in \{1, ..., N\}$
for $i \in \{1, ..., N\}$ ▷ iterate driving points
  for $j \in \{1, ..., n_M\}$ ▷ iterate added masses
    $\Delta G^{ij} \leftarrow T_O \left[\tilde{G}^{ij}_{:z} - \tilde{G}_{:z}\right]$
    $G^{ij}_M \leftarrow M_j T^i_O \tilde{G}^{ij}_{yiz}$
  end for
  $G_{:u_i} \leftarrow \left[\Delta G^{i1} \quad \dots \quad \Delta G^{in_M}\right] \left[G^{i1}_M \quad \dots \quad G^{in_M}_M\right]^+$ ▷ Equation (16)
end for
$G \leftarrow \left[G_{:z} \quad G_{:u_1} \quad \dots \quad G_{:u_N}\right]$

Procedure 3 AMPIE Parametric

Input: $G_{:z}$, $G^{ij}_{:z} \forall i \in \{1, ..., N\}, j \in \{1, ..., n_M\}$, and order n
Output: G with $G_{:u_i} \forall i \in \{1, ..., N\}$
Identify $\{A, B_{:z}, C, D_{:z}\} \leftarrow G_{:z}$, enforce $D_{:z} = CA^{-1}B_{:z}$
for $i \in \{1, ..., N\}$ ▷ iterate coupling points
  for $j \in \{1, ..., n_M\}$ ▷ iterate added masses
    for $\omega_k \in \Omega$
      $A^{\blacksquare}_{ij} \leftarrow A^{\blacksquare}_{ij} + \Delta A^{\blacksquare}_{ij}(\omega_k)$ ▷ Equation (25)
      $b^{\blacksquare}_{ij} \leftarrow b^{\blacksquare}_{ij} + \Delta b^{\blacksquare}_{ij}(\omega_k)$ ▷ Equation (26)
    end for
    $A^{\blacksquare}_i \leftarrow A^{\blacksquare}_i + A^{\blacksquare}_{ij}$, $b^{\blacksquare}_i \leftarrow b^{\blacksquare}_i + b^{\blacksquare}_{ij}$ ▷ Equation (27)
  end for
  $B_{:u_i} \leftarrow \left(A^{\blacksquare}_i\right)^{-1} b^{\blacksquare}_i$ ▷ Equation (28)
  $G_{:u_i} \leftarrow C\Lambda(\omega)B_{:u_i}$
end for
$B \leftarrow \left[B_{:z} \quad B_{:u_1} \quad \dots \quad B_{:u_N}\right]$
$D \leftarrow CA^{-1}B$
$G \leftarrow \{A, B, C, D\}$

B AMPIE and MUM

In the previously proposed methods [23, 11, 12], the mass uncoupling method is formulated on a scalar basis. In order to clarify the basic steps, the items in Equation (5) are chosen to yield the simplest scenario where only scalar channels are considered. The key assumption for the mathematical steps is that one mass is assumed to solely act in one translational direction:

$$G^1 = \begin{bmatrix} G^1_{pz} & G^1_{pu} \\ G^1_{yz} & G^1_{yu} \end{bmatrix} \in \mathbb{C}^{2\times 2}, G = \begin{bmatrix} G_{pz} & G_{pu} \\ G_{yz} & G_{yu} \end{bmatrix} \in \mathbb{C}^{2\times 2} \tag{B.1}$$

$$\boldsymbol{M}_1 = \begin{bmatrix} 0 & 0 \\ 0 & m \end{bmatrix} \in \mathbb{R}^{2\times 2}, T_I = \begin{bmatrix} 0 \\ 1 \end{bmatrix}, T_O = \begin{bmatrix} 0 & 1 \end{bmatrix}. \tag{B.2}$$

Then, Equation (5) becomes

$$\begin{bmatrix} G^1_{pz} & G^1_{pu} \\ G^1_{yz} & G^1_{yu} \end{bmatrix} = \left[\begin{bmatrix} 1 & 0 \\ 0 & 1 \end{bmatrix} - \begin{bmatrix} 0 & G_{pu}m \\ 0 & G_{yu}m \end{bmatrix}\right]^{-1} \begin{bmatrix} G_{pz} & G_{pu} \\ G_{yz} & G_{yu} \end{bmatrix}. \tag{B.3}$$

where G_{pu} and G_{yu} are unknown. The scalar formulation allows the inverse to be calculated:

$$\begin{bmatrix} G^1_{pz} & G^1_{pu} \\ G^1_{yz} & G^1_{yu} \end{bmatrix} = \begin{bmatrix} 1 & \frac{G_{pu}m}{1-G_{yu}m} \\ 0 & \frac{1}{1-G_{yu}m} \end{bmatrix} \begin{bmatrix} G_{pz} & G_{pu} \\ G_{yz} & G_{yu} \end{bmatrix} = \begin{bmatrix} G_{pz} + \frac{G_{pu}mG_{yz}}{1-G_{yu}m} & G_{pu} + \frac{G_{pu}mG_{yu}}{1-G_{yu}m} \\ \frac{G_{yz}}{1-G_{yu}m} & \frac{G_{yu}}{1-G_{yu}m} \end{bmatrix}, \tag{B.4}$$

and the equations

$$G^1_{yz} = \frac{G_{yz}}{1 - G_{yu}m} \Rightarrow G_{yu} = \frac{1 - \frac{G_{yz}}{G^1_{yz}}}{m} = \frac{G^1_{yz} - G_{yz}}{mG^1_{yz}} \tag{B.5}$$

$$G^1_{pz} = G_{pz} + \frac{G_{pu}mg_{yz}}{1 - G_{yu}m} = G_{pz} + G_{pu}mG^1_{yz} \Rightarrow G_{pu} = \frac{G^1_{pz} - G_{pz}}{mG^1_{yz}} \tag{B.6}$$

are obtained. Using the same assumptions and Equation (6) one finds:

$$G^1 - G = GM_1G^1 \tag{B.7}$$

$$\begin{bmatrix} G^1_{pz} & G^1_{pu} \\ G^1_{yz} & G^1_{yu} \end{bmatrix} - \begin{bmatrix} G_{pz} & G_{pu} \\ G_{yz} & G_{yu} \end{bmatrix} = \begin{bmatrix} G_{pz} & G_{pu} \\ G_{yz} & G_{yu} \end{bmatrix} \begin{bmatrix} 0 & 0 \\ 0 & m \end{bmatrix} \begin{bmatrix} G^1_{pz} & G^1_{pu} \\ G^1_{yz} & G^1_{yu} \end{bmatrix} \tag{B.8}$$

$$\begin{bmatrix} G^1_{pz} \\ G^1_{yz} \end{bmatrix} - \begin{bmatrix} G_{pz} \\ G_{yz} \end{bmatrix} = \begin{bmatrix} G_{pu} \\ G_{yu} \end{bmatrix} mG^1_{yz} \Rightarrow \begin{bmatrix} G_{pu} \\ G_{yu} \end{bmatrix} = \begin{bmatrix} \frac{G^1_{pz} - G_{pz}}{mG^1_{yz}} \\ \frac{G^1_{yz} - G_{yz}}{mG^1_{yz}} \end{bmatrix} \tag{B.9}$$

Naturally, both procedures yield the same results. However, the steps (B.4) - (B.6) are arguably more cumbersome than the steps (B.7) - (B.9). Still, the main benefit of Equations (B.7) - (B.9) becomes apparent when the assumption of a scalar mass is dropped. In that case, the inverse in Equation (B.3) becomes $\left[\begin{bmatrix} I & 0 \\ 0 & I \end{bmatrix} - \begin{bmatrix} 0 & G_{pu}M \\ 0 & G_{yu}M \end{bmatrix}\right]^{-1}$ where $G_{yu} \in \mathbb{C}^{6\times 6}$ accommodates a six dimensional coupling point. Note that the quantities G_{pu} and G_{yu} are the unknown quantities that are supposed to be calculated. A straightforward, numerical matrix-inversion is, therefore, not possible. As the dimension increases, the required symbolic inversion would result in far more complex expressions which are not as conveniently solvable as (B.4) - (B.6). In addition, no such formulation is known to the author. As these hurdles are entirely avoided in the expression (B.7) - (B.9) the formalism is considered to be more flexible as arbitrary interface dimensions and constraints can be applied, and multiple masses can be considered due to the LES-based solution.

C Results

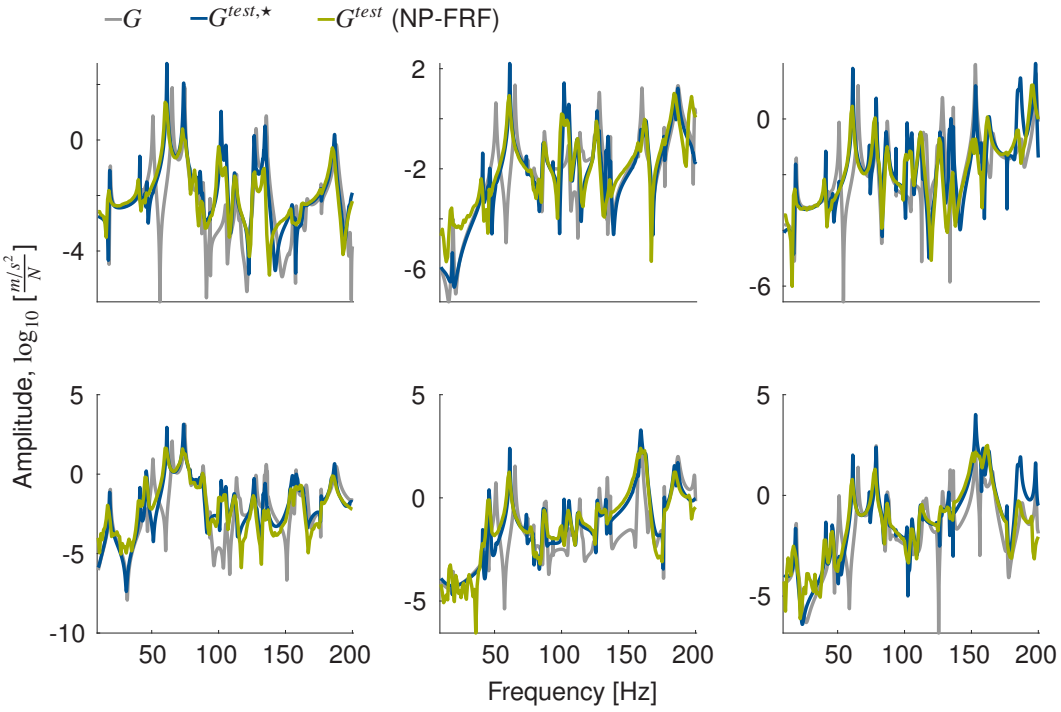

Fig. C.1: AMPIE test prediction for channel $[p_2, p_6] \leftarrow [z_1, z_2, z_3]$: default system as well as measured and predicted test-combination including the added test-channel z_3.

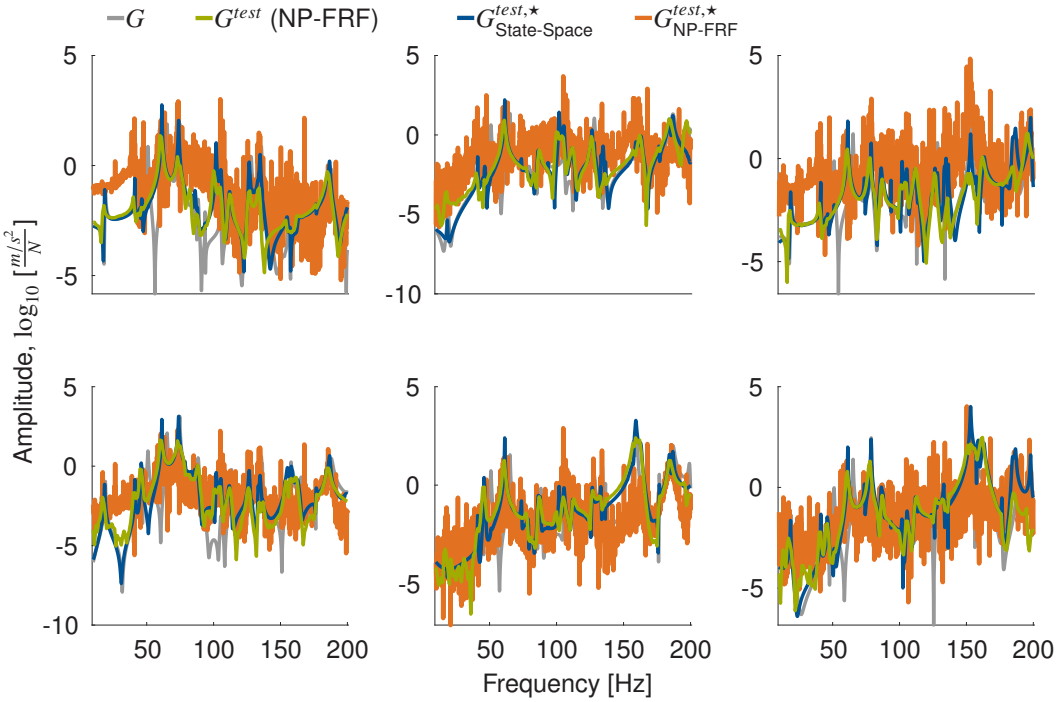

Fig. C.2: Shows the same information as Figure C.1, including the results from the NP-FRF-based AMPIE procedure. Note that $G^{test,\star}_{\text{State-Space}}$ refers to the state-space-based AMPIE approach in Equation (27), whereas $G^{test,\star}_{\text{NP-FRF}}$ refers to the non-parametric approach (16) and G^{test} (NP-FRF) emphasizes that the data is a non-parametric FRF.

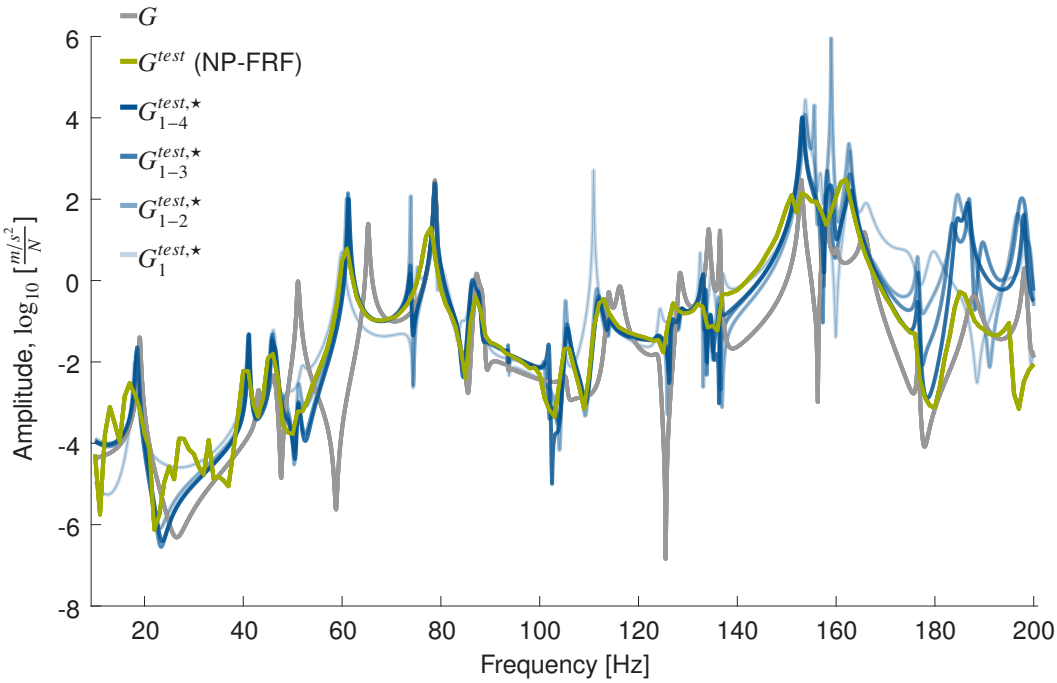

Fig. C.3: AMPIE test-prediction for channel $[p_2] \leftarrow [z_3]$: default system as well as measured and predicted test-combination including the added test-channel z_3 based on estimated systems with one to four added masses.

D Constraint

System identification in structural mechanics mostly uses accelerations as outputs, i.e. $G_a = C_a\Lambda(\omega)B + D_a$ with $D_a \neq 0$, but where $D_a = C_aA^{-1}B$ is not automatically fulfilled for standard identification algorithms. However, to derive a method to ensure the feedthrough-constraint $D_a = C_aA^{-1}B$ for acceleration outputs, starting from displacements is more suitable. If a state-space system $G_d = C_d\Lambda(\omega)B + D_d$ describes displacements or velocities as outputs, described by index d or v respectively, the feedthrough D_d or D_v is supposed to be zero, whereas D_a is non-zero. This can be observed by transforming a second-order model $M\ddot{q} + C\dot{q} + Kq = B'u, \;\; y = C'q$ into a first-order model $\dot{x} = Ax + Bu, \;\; y = C_dx$:

$$\underbrace{\begin{bmatrix}\dot{q}\\ \ddot{q}\end{bmatrix}}_{\dot{x}} = \underbrace{\begin{bmatrix}0 & I\\ -M^{-1}K & -M^{-1}C\end{bmatrix}}_{A}\underbrace{\begin{bmatrix}q\\ \dot{q}\end{bmatrix}}_{x} + \underbrace{\begin{bmatrix}0\\ -M^{-1}B'\end{bmatrix}}_{B}u, \;\; y = \underbrace{\begin{bmatrix}C' & 0\end{bmatrix}}_{C_d}\underbrace{\begin{bmatrix}q\\ \dot{q}\end{bmatrix}}_{x} \tag{D.1}$$

where $D_d = 0$. Deriving $y = C'q$ with respect to time, one finds $\dot{y} = C'\dot{q}$ which shows that D_v has to be zero as well. For the first-order model, this results in the following expressions:

$$y = C_dx \Rightarrow \dot{y} = C_d\dot{x} \Rightarrow \dot{y} = C_d\left(Ax + Bu\right) = C_dAx + \underbrace{C_dB}_{D_v}u \Rightarrow D_v = C_dB = 0 \tag{D.2}$$

$$\ddot{y} = C_dA\dot{x} = \underbrace{C_dA^2}_{C_a}x + \underbrace{C_dAB}_{D_a}u = 0 \Rightarrow C_d = C_aA^{-2}, \;\; D_a = C_dAB = C_aA^{-1}B \tag{D.3}$$

Summarizing, starting from displacement outputs with $D_d = 0$ and deriving the system with respect to time, one finds that $D_v = C_dB \overset{!}{=} 0$ and $C_d = C_aA^{-2}$ resulting in

$$C_aA^{-2}B = 0 \tag{D.4}$$

which is a sufficient condition to ensure that $D_a = C_aA^{-1}B$. However, Equation (D.4) allows to exploit the fact that, if $n > n_I$ which would be the case for the vast majority of all AMPIE applications, a nullspace $N \in \mathbb{R}^{(n-n_I)\times n}$ exists such that $NA^{-2}B = 0$. The matrix C_a can then be defined by a linear combination in that nullspace $C_a \overset{!}{=} PN$ where $P \in \mathbb{R}^{n_O\times(n-n_I)}$ is unknown. There are two main possibilities to determine P. First, one could directly solve the required equations on matrix-level by inserting $C_a \overset{!}{=} PN$ in Equation (D.4), or second, P can be determined such that the resulting FRF $G_{\text{cstr}}(\omega)$ with substituted quantities C_a and D_a matches the FRF $G_a(\omega)$ of the original system as good as possible. The latter foregoing is chosen as it allows to exclude frequency-intervals where out-of-band modes are located.

Mathematically, this means that $G_{\text{cstr}}(\omega) = C_a\Lambda(\omega)B + C_aA^{-1}B = PN\Lambda(\omega)B + PNA^{-1}B = P\left[N\Lambda(\omega)B + NA^{-1}B\right] = P\bar{\Lambda}(\omega)$, equals the FRF $G_a(\omega) = C_a\Lambda(\omega)B + D_a$. Given a frequency grid Ω, this results in

$$G_{\text{cstr}}(\omega_k) = P\bar{\Lambda}(\omega_k) \overset{!}{=} C_a\Lambda(\omega_k)B + D_a = G_a(\omega_k) \qquad \forall\omega_k \in \Omega \in \mathbb{R}^{n_\omega} \tag{D.5}$$

which can be converted into and solved by a LES of the form

$$\begin{bmatrix}P\bar{\Lambda}(\omega_1) & \dots & P\bar{\Lambda}(\omega_{n_\omega})\end{bmatrix} = \begin{bmatrix}G_a(\omega_1) & \dots & G_a(\omega_{n_\omega})\end{bmatrix} \tag{D.6}$$

$$P\begin{bmatrix}\bar{\Lambda}(\omega_1) & \dots & \bar{\Lambda}(\omega_{n_\omega})\end{bmatrix} = \begin{bmatrix}G_a(\omega_1) & \dots & G_a(\omega_{n_\omega})\end{bmatrix} \tag{D.7}$$

$$\begin{bmatrix}\bar{\Lambda}^{\mathsf{T}}(\omega_1)\\ \vdots\\ \bar{\Lambda}^{\mathsf{T}}(\omega_{n_\omega})\end{bmatrix}P^{\mathsf{T}} = \begin{bmatrix}G_a^{\mathsf{T}}(\omega_1)\\ \vdots\\ G_a^{\mathsf{T}}(\omega_{n_\omega})\end{bmatrix}. \tag{D.8}$$

Authors' Contributions

Benjamin Kammermeier put forward the theoretical derivation of the outlined AMPIE approach, conducted the experiments to test the approach, and wrote the first draft of the manuscript. Johannes Mayet supervised the theoretical work. Daniel J. Rixen supervised the work and supported the research by providing the testing equipment and manufacturing capabilities to conduct the required experiments. All authors reviewed and edited the final manuscript.

References

[1] J. Harvie and P. Avitabile. Effects of Precise FRF Measurements for Frequency Based Substructuring. In R. Mayes, D. Rixen, and M. Allen, editors, *Topics in Experimental Dynamic Substructuring, Volume 2*, pages 277–285, New York, NY, 2014. Springer New York. ISBN 978-1-4614-6540-9. doi:10.1007/978-1-4614-6540-9_22.

[2] J. O'Callahan, P. Avitabile, and R. Riemer. System Equivalent Reduction Expansion Process (SEREP). In *Proceedings of the VII international modal analysis conference (IMAC)*, volume 1, pages 29–37, Boston, MA, 1989.

[3] L. Thibault, A. Butland, and P. Avitabile. Variability Improvement of Key Inaccurate Node Groups – VIKING. In R. Allemang, J. De Clerck, C. Niezrecki, and J. Blough, editors, *Topics in Modal Analysis II, Volume 6*, pages 603–624, New York, NY, 2012. Springer New York. ISBN 978-1-4614-2419-2. doi:10.1007/978-1-4614-2419-2_61.

[4] S. W. Klaassen, M. V. van der Seijs, and D. de Klerk. System equivalent model mixing. *Mechanical Systems and Signal Processing*, 105:90–112, 2018. ISSN 0888-3270. doi:https://doi.org/10.1016/j.ymssp.2017.12.003.

[5] S. W. Klaassen and M. V. van der Seijs. Introducing SEMM: A Novel Method for Hybrid Modelling. In A. Linderholt, M. S. Allen, R. L. Mayes, and D. Rixen, editors, *Dynamics of Coupled Structures, Volume 4*, pages 117–125. Springer International Publishing, 2018. ISBN 978-3-319-74654-8. doi:10.1007/978-3-319-74654-8_10.

[6] N. M. M. Maia and T. A. N. Silva. An expansion technique for the estimation of unmeasured rotational frequency response functions. *Mechanical Systems and Signal Processing*, 2021. ISSN 0888-3270. doi:https://doi.org/10.1016/j.ymssp.2021.107634.

[7] M. I. Friswell and J. E. T. Penny. Updating model parameters from frequency domain data via reduced order models. *Mechanical Systems and Signal Processing*, 4(5):377–391, 1990. ISSN 0888-3270. doi:https://doi.org/10.1016/0888-3270(90)90064-R.

[8] J. E. Mottershead and M. I. Friswell. Model Updating In Structural Dynamics: A Survey. *Journal of Sound and Vibration*, 167 (2):347–375, 1993. ISSN 0022-460X. doi:https://doi.org/10.1006/jsvi.1993.1340.

[9] M. I. Friswell and J. E. Mottershead. *Finite Element Model Updating in Structural Dynamics*, volume 38 of *Solid Mechanics and its Applications*. Springer Netherlands, Dordrecht, 1995. ISBN 978-90-481-4535-5. doi:10.1007/978-94-015-8508-8.

[10] C. Yasuda, P. J. Riehle, D. L. Brown, and R. J. Allemang. An estimation method for rotational degrees of freedom using a mass additive technique. 1984.

[11] J. M. M. Silva and A. M. R. Ribeiro. Some Applications of Coupling/Uncoupling Techniques in Structural Dynamics. Part 3: Estimation of Rotational Frequency-Response-Functions using MUM. 1997.

[12] J. M. M. Silva, N. M. M. Maia, and A. M. R. Ribeiro. Cancellation of Mass-Loading Effects of Transducers and Evaluation of Unmeasured Frequency Response Functions. *Journal of Sound and Vibration*, 236(5):761–779, 2000. ISSN 0022-460X. doi:https://doi.org/10.1006/jsvi.1999.2993.

[13] J. E. Mottershead, A. Kyprianou, and H. Ouyang. Structural modification. Part 1: rotational receptances. *Journal of Sound and Vibration*, 284(1):249–265, 2005. ISSN 0022-460X. doi:https://doi.org/10.1016/j.jsv.2004.06.021.

[14] M. S. Allen, R. L. Mayes, and E. J. Bergman. Experimental modal substructuring to couple and uncouple substructures with flexible fixtures and multi-point connections. *Journal of Sound and Vibration*, 329(23):4891–4906, 2010. ISSN 0022-460X. doi:https://doi.org/10.1016/j.jsv.2010.06.007.

[15] R. L. Mayes. Tutorial on Experimental Dynamic Substructuring Using the Transmission Simulator Method. In R. Mayes, D. Rixen, D. Griffith, D. De Klerk, S. Chauhan, et al., editors, *Topics in Experimental Dynamics Substructuring and Wind Turbine Dynamics, Volume 2*, pages 1–9, New York, NY, 2012. Springer New York. ISBN 978-1-4614-2422-2. doi:10.1007/978-1-4614-2422-2_1.

[16] M. L. M. Duarte and D. J. Ewins. Rotational Degrees of Freedom for Structural Coupling Analysis via Finite-Difference Technique with Residual Compensation. *Mechanical Systems and Signal Processing*, 14(2):205–227, 2000. ISSN 0888-3270. doi:https://doi.org/10.1006/mssp.1999.1241.

[17] A. S. Elliott, A. T. Moorhouse, and G. Pavić. Moment excitation and the measurement of moment mobilities. *Journal of Sound and Vibration*, 331(11):2499–2519, 2012. ISSN 0022-460X. doi:https://doi.org/10.1016/j.jsv.2012.01.022.

[18] M. V. van der Seijs. *Experimental Dynamic Substructuring*. PhD thesis, Delft University of Technology, 2016.

[19] T. Bregar, N. Holeček, G. Čepon, D. J. Rixen, and M. Boltežar. Including directly measured rotations in the virtual point transformation. *Mechanical Systems and Signal Processing*, 141:106440, 2020. ISSN 0888-3270. doi:https://doi.org/10.1016/j.ymssp.2019.106440.

[20] M. A. Sanderson and C. R. Fredö. Direct measurement of moment mobility: Part I: A theoretical study. *Journal of Sound and Vibration*, 179(4):669–684, 1995. ISSN 0022-460X. doi:https://doi.org/10.1006/jsvi.1995.0043.

[21] M. A. Sanderson. Direct measurement of moment mobility: Part II: An experimental study. *Journal of Sound and Vibration*, 179(4):685–696, 1995. ISSN 0022-460X. doi:https://doi.org/10.1006/jsvi.1995.0044.

[22] S. Jianxin and C. M. Mak. Direct measurement of moment mobility and a moment excitation system. *Applied Acoustics*, 63 (2):139–151, 2002. ISSN 0003-682X. doi:https://doi.org/10.1016/S0003-682X(01)00030-5.

[23] N. M. M. Maia, J. M. M. Silva, and A. M. R. Ribeiro. Some applications of coupling/uncoupling techniques in structural dynamics. Part 2: Generation of the whole FRF matrix from measurements on a single column: The mass uncoupling method (MUM). 1997.

[24] D. Montalvão, T. Baker, B. Ihracska, and M. Aulaqi. A generalised multiple-mass based method for the determination of the live mass of a force transducer. *Mechanical Systems and Signal Processing*, 83:506–521, 2017. ISSN 08883270. doi:10.1016/j.ymssp.2016.06.028.

[25] N. Hosoya, S. Yaginuma, H. Onodera, and T. Yoshimura. Estimation of the auto frequency response function at unexcited points using dummy masses. *Journal of Sound and Vibration*, 337:14–27, 2015. ISSN 0022-460X. doi:https://doi.org/10.1016/j.jsv.2014.09.033.

[26] D. J. Ewins. On predicting point mobility plots from measurements of other mobility parameters. *Journal of Sound and Vibration*, 70(1):69–75, 1980. ISSN 0022-460X. doi:https://doi.org/10.1016/0022-460X(80)90554-4.

[27] A. T. Moorhouse and A. S. Elliott. The “round trip” theory for reconstruction of Green’s functions at passive locations. *The Journal of the Acoustical Society of America*, 134(5):3605–3612, 11 2013. ISSN 0001-4966. doi:10.1121/1.4821210.

[28] J. Lunze. *Regelungstechnik 1*. Springer-Lehrbuch. Springer Berlin Heidelberg, Berlin, Heidelberg, 2010. ISBN 978-3-642-13807-2. doi:10.1007/978-3-642-13808-9.

[29] L. Ljung. *System Identification*, pages 163–173. Birkhäuser Boston, Boston, MA, 1998. ISBN 978-1-4612-1768-8. doi:10.1007/978-1-4612-1768-8_11.

[30] T. McKelvey, H. Akcay, and L. Ljung. Subspace-based multivariable system identification from frequency response data. *IEEE Transactions on Automatic Control*, 41(7):960–979, jul 1996. ISSN 00189286. doi:10.1109/9.508900.

[31] L. Ljung. Perspectives on system identification. *Annual Reviews in Control*, 34(1):1–12, apr 2010. ISSN 13675788. doi:10.1016/j.arcontrol.2009.12.001.

[32] D. J. Ewins. *Modal Testing: Theory, Practice and Application, 2md Edition*. 2009. ISBN 978-0-863-80218-8.

[33] P. Avitabile. *Modal Testing: A Practitioner’s Guide*. John Wiley & Sons Ltd, 2017. ISBN 9781119222989. doi:10.1002/9781119222989.

[34] P. Sjövall and T. J. S. Abrahamsson. Component system identification and state-space model synthesis. *Mechanical Systems and Signal Processing*, 21(7):2697–2714, 2007. ISSN 0888-3270. doi:https://doi.org/10.1016/j.ymssp.2007.03.002.

[35] M. Gibanica and T. J. S. Abrahamsson. Identification of physically realistic state-space models for accurate component synthesis. *Mechanical Systems and Signal Processing*, 145:106906, 2020. ISSN 08883270. doi:10.1016/j.ymssp.2020.106906.

[36] M. Géradin and D. J. Rixen. *Mechanical Vibrations: Theory and Application to Structural Dynamics, 3rd Edition*. 2015. ISBN 978-1-118-90020-8.

[37] Y. Ren and C. F. Beards. Identification of joint properties of a structure using frf data. *Journal of Sound and Vibration*, 186(4): 567–587, 1995. ISSN 0022-460X. doi:https://doi.org/10.1006/jsvi.1995.0469.

[38] W. E. Larimore. Canonical variate analysis in identification, filtering, and adaptive control. In *29th IEEE Conference on Decision and Control*, pages 596–604 vol.2, 1990. doi:10.1109/CDC.1990.203665.

[39] The MathWorks Inc. MATLAB R2018b System Identification Toolbox.

[40] R. B. Blackman and J. W. Tukey. The measurement of power spectra from the point of view of communications engineering — Part I. *The Bell System Technical Journal*, 37(1):185–282, 1958. doi:10.1002/j.1538-7305.1958.tb03874.x.

[41] P. W. Holland and R. E. Welsch. Robust regression using iteratively reweighted least-squares. *Communications in Statistics - Theory and Methods*, 6(9):813–827, 1977. doi:10.1080/03610927708827533.

[42] J. O. Street, R. J. Carroll, and D. Ruppert. A Note on Computing Robust Regression Estimates via Iteratively Reweighted Least Squares. *The American Statistician*, 42(2):152–154, 1988. doi:10.1080/00031305.1988.10475548.